Evaluation of Alkaline Sodium Silicate Gel for Reservoir In-Depth Profile Modifications to Enhance Water Sweep Efficiency in Sandstone Reservoirs

by

Hossein Ali Akhlaghi Amiri

Thesis submitted in partial fulfillment of
the requirements for the degree of
DOCTOR OF PHILOSOPHY
(PhD)

Faculty of Science and Technology
Department of Petroleum Engineering
2014

University of Stavanger
N-4036 Stavanger
NORWAY
www.uis.no

ISBN: 978-82-7644-563-3
ISSN: 1890-1387

PhD Thesis No. 221

PREFACE

This thesis is submitted in partial fulfillment of the requirements for the degree of PhD (Doctor of Philosophy) in Petroleum Engineering at University of Stavanger, Norway. The thesis presents the results of the research work conducted at Department of Petroleum Engineering, University of Stavanger (UiS) from April 2011. The outcome of this study is given through 3 published papers, one manuscript under review and one conference paper which are attached at the end of the thesis.

An overview of the work is given in introduction, followed by the objectives of the work in section two. Materials, used methods and different numerical approaches employed in this study are in section three, followed by the results and discussion section. Conclusions and recommendations are given in the last section. All the cited references are given in section six.

ABSTRACT

Alkaline sodium silicate (Na-silicate) is addressed to be applied for in-depth water conformance control in sandstone reservoirs containing high permeability layers.

The main factors affecting the gel time, strength and shrinkage in the alkaline silicate systems are the Na-silicate content, the pH, the presence of divalent ions and temperature. Divalent ions, e.g., Ca^{2+} and Mg^{2+}, reduced the gel time and increased the gel strength and shrinkage. They also caused metal silicate precipitation at high concentrations. No precipitation formed with low-salinity water (25-times diluted seawater), which makes it a possible option for pre-flushing reservoir in field application.

Temperature accelerated the gel time but the gel strength was shown to be reduced as temperature increased from 20 to 50 °C. Further increase in the temperature to 80 °C showed a slight increase of the gel strength. This may be attributed to increase of silicate solubility at high temperature. High shear rates, even for a short interval before gelation (which resembles the wellbore case), accelerated gel time; hence must be considered in field applications. A simple graphical method was suggested to estimate the combined effects of different factors on the gel time and strength.

Dynamic adsorption of silicate in sand-packs was considerably lower than the estimated mono-layer adsorption. It was demonstrated that silicate adsorption is reversible, and most of the adsorbed mass is desorbed in the post-flush water. Na-silicate showed water-like injectivity in flooding experiments.

In the name of Allah

To my family; especially my kind mother and my lovely wife
for all their supports and motivations

and

In memory of Imam Ali (Peace be upon him)

ACKNOWLEDGEMENTS

First and foremost I praise God, the almighty for supporting me through my entire life, providing me this opportunity and granting me the capability to proceed successfully.

I would like to extend my profound gratitude to Professor Aly A. Hamouda for excellent supervision during my PhD program and for providing interesting comments, ideas and encouragements. I appreciate all advantages that I have received from him.

I gratefully acknowledge Dong Energy Company, Norway for the financial support of this project. I would like to thank Kelly Tyler, Lars G. Gammelgaard and Oddbjørn Melberg from Dong Energy Company, for their technical follow up and interest during my PhD.

I would like to thank Inger Johanne Munthe-Kaas Olsen for her positive attitude and great assistance in getting the chemicals used in this work and Kim Andre Nesse Vorland and Ola Ketil Siqveland for technical supports in performing the experiments.

I would like to express my best appreciation to the University of Stavanger and its staff. I would like to thank Elisabeth Stornes Fiskå for her excellent arrangements in administrative affairs and Kathrine Molde for her kindness and helps during my PhD and all my colleagues at the Department of Petroleum Engineering, University of Stavanger for their support.

I express my sincere gratitude to my friends in Stavanger for their motivation and encouragements.

The last but not least, I revere my family for all their support and encouragement. I am forever indebted to my mother who raised me with love and supported me in all my pursuits. And most of all for my loving, supportive, encouraging, and patient wife 'Sima', whose faithful support during different stages of this PhD is appreciated. Thank you.

Hossein Akhlaghi

Feb 2014

Stavanger, Norway

LIST OF PUBLICATIONS

I. **H. A. Akhlaghi Amiri and A. A. Hamouda,** 2013: Evaluation of level set and phase field methods in modeling two phase flow with viscosity contrast through dual-permeability porous medium. *International Journal of Multiphase flow*. 52, 22-34.

II. **H. A. Akhlaghi Amiri and A. A. Hamouda,** 2014: Pore-scale modeling of non-isothermal two phase flow in 2D porous media: Influences of viscosity, capillarity, wettability and heterogeneity. *International Journal of Multiphase flow*. 61, 14-27.

III. **A. A. Hamouda and H. A. Akhlaghi Amiri,** 2014: Factors affecting alkaline sodium silicate gelation for in-depth reservoir profile modification. *Energies*. 7 (2), 568-590.

IV. **H. A. Akhlaghi Amiri and A. A. Hamouda,** 2012: Pore-scale simulation of coupled two-phase flow and heat transfer through dual-permeability porous medium. Presented at 2012 COMSOL Conference, Milan, Italy, October 10-12.

V. **H. A. Akhlaghi Amiri, A. A. Hamouda and A. Roostaei,** 2014: Sodium silicate behavior in porous media being applied for in-depth profile modifications (under review).

TABLE OF CONTENTS

LIST OF FIGURES

LIST OF TABLES

NOMENCLATURE

A	pre-exponential factor (min, h)
A_{ext}	external area (m^2)
C	concentration (mg/l, mol/l, wt%)
C_o	initial concentration (mg/l, wt%)
Ca	capillary number
Cn	Cahn number
C_p	heat capacity (Btu/ft^3F)
D_q	grain diameter (m)
D_t	throat diameter (m)
E_a	activation energy (J/mol)
F	force (N)
F_{rr}	residual resistance factor
G	chemical potential
h	high permeability layer thickness (ft, m)
H	thickness of porous medium (ft, m)
k	permeability (md, d)
k_r	relative permeability
L	length of porous medium (ft, m)
l_c	characteristic length (m)
M	viscosity ratio
n	molar ratio
p	pressure (kPa, psi)
R	universal ideal gas constant (8.314 J/mol K)
s_w	water saturation
s_{wc}	connate water saturation
s_{or}	residual oil saturation
SR	shear rate (s^{-1})
T	temperature (^oC, F, K)
t	time (s, min, h)
t_g	gelation time (min, h)
t_{g0}	gelation time at room temperature and zero salinity (min, h)
t_{mgs}	maximum gel strength time (min, h)
u	velocity (m/s)
V	volume (m^3)
W	width of porous medium (ft, m)
$wt\%$	weight percent
x	distance in the flow direction (ft, m)

Greeks

γ	diffusion coefficient, mobility (m^2/s)
γ_c	characteristic mobility (m^2/s)
ε	interfacial thickness parameter (m)
θ_c	contact angle (degree, radian)
κ	thermal conductivity (Btu/ft.day.F)
λ	mixing energy density (J/m^3)
μ	viscosity (cp, Pa·s)
ρ	density (kg/m^3, lbm/ft^3)
σ	interfacial tension (N/m, mN/m)
ϕ	phase field order parameter
ψ	auxiliary parameter

Subscripts

h	horizontal direction
inj	injection
Na-s	sodium silicate
max	maximum
o	oil
T	temperature
v	vertical direction
w	water
x	x direction
y	y direction

Abbreviations

ACS	American Chemical Society
AMR	Adaptive Mesh Refinement
ASTM	American System of Testing and Materials
BDF	Backward Differentiation Formula
CMG	Computer Modelling Group
DLVO	Derjaguin, Landau, Verway, Overbeek
DW	Distilled Water
EOR	Enhanced Oil Recovery
HP	High Permeability
HPAM	Hydrolyzed Polyacrylamide
ICP	Inductively Coupled Plasma
LP	Low Permeability
LSM	Level Set Method
LSW	Low Salinity Water
Na-silicate	Sodium Silicate
NN-DMDA	N,N-dimethyldodecylamine
n-C10	Normal Decane
OOIP	Oil Originally In Place
PFM	Phase Field Method
PPG	Preformed Particle Gel
PV	Pore Volume
RF	Recovery Factor
SSW	Synthetic Sea Water

1. INTRODUCTION

Nowadays, extending the life of depleted hydrocarbon reservoirs has become a real challenge, due to the growing demands for the fossil fuels. One of the main concerns in mature oil reservoirs is excessive water production (Ogunberu and Asghari, 2006). Produced excess water deteriorates the profitability of the production operations in an oil field. Because on one hand, it affects volumetric sweep efficiency of oil and hence drastically reduces oil production rate (Sydansk and Romero-Zenom, 2011). On the other hand, production of a certain volume of water requires equal or even more energy than the same volume of oil (Eoff et al., 2007). Moreover, the large amount of the produced water imposes additional costs for separation, disposal, handling and also managing other related difficulties such as sand control, tubular corrosion, higher tendency for scale formation and so on (Sydansk and Southwell, 2000; Ogunberu and Asghari, 2006; Nasr-El-Din and Taylor, 2005; Eoff et al., 2007).

Poor water sweep efficiency and early water breakthrough are caused by water-oil displacement instabilities, including channeling and viscous fingering (Ferer et al., 2004; Bai et al., 2007). These instabilities originate mainly by the reservoir heterogeneities, e.g., high permeability streaks and fractures, and unfavorable fluids' mobility ratio (Frette et al., 1997; Bai et al., 2007; Seright et al., 2011). Enhancing oil recovery in such reservoirs demands a method to control the injected water behavior in the porous media.

1.1. Water conformance control

Conformance control treatments are referred to those which serve to improve volumetric sweep efficiency during oil-recovery flooding operations and also those which are used to minimize excess water production (Sydansk and

Southwell, 2000; Sydansk, 2007; Sydansk and Romero-Zenom, 2011). The application of effective conformance control treatments has always been an elusive goal in the oil industry since the 60s, when the necessity to control flow profiles in the producing reservoirs was first recognized (Sydansk and Southwell, 2000; Lakatos and Lakatos-Szabo, 2012). Since then, a great variety of water control methods have been proposed.

Conformance control methods can be generally divided into mechanical and chemical methods (Prada et al., 2000; Kabir, 2001). Mechanical methods, such as tubing patch, scab liner and cement squeeze, form a seal in wells and near wellbore areas to control water production (Kabir, 2001). Mechanical methods, in general, require work over rigs which make the process too expensive (Nasr-El-Din and Taylor, 2005). While chemical methods provide cheaper as well as more effective means for water conformance control (Kabir, 2001).

1.1.1. Chemical-based conformance control methods

During the last half century, different types of chemical methods have been developed and applied for water control, such as cross-linked polymer gels (Sydansk, 1990; Mack and Smith, 1994; Moradi-Araghi, 1994; Manrique et al., 2007), resins and elastomers (Nagra et al., 1986; Seright and Martin, 1993; Zhuang et al., 1997; Kabir, 2001), chemical precipitates (Lakatos and Lakatos-szabo, 1996; Lakatos et al., 2002; Kosztin et al., 2002; Nasr-El-Din et al., 2004) and inorganic silica gel-based systems (Smith et al., 1969; Krumrine and Boyce, 1985; Vinot et al., 1989; Jurinak and Summerss, 1991; Islam and Farouq Ali, 1993). Among them, cross-linked polymer and silica gels have been the most popular and effective methods for water conformance control (Krumrine and Boyce, 1985; Manrique et al., 2007).

Cross-linked polymer gel system is a mixture of two components, high molecular weight polymer and low molecular weight cross-linker (Schechter, 1992). Under certain conditions, e.g., high temperature, cross-linker molecules make chemical bonds between polymer molecules, which results in a three dimensional tangle of the interconnected molecules. The most widely used polymer in enhanced oil recovery applications is hydrolyzed Poly-acrylamide, HPAM (Nasr-El-Din and Taylor, 2005; Manrique et al., 2007) and the popular cross-linkers are either metal ions, such as Al^{3+} and Cr^{3+} (Mack and Smith, 1994; Sydansk, 1990, 1993) or organic materials, such as phenol and formaldehyde (Hardy et al., 1999; Prada et al., 2000; Moradi-Araghi, 1994). Bright Water is an in-situ cross-linked polymer gel which is thermally activated (Frampton et al., 2004; Pritchett et al., 2003). Preformed gel systems, such as PPG, are also categorized as cross-linked polymer gels (Bai et al., 2007; Zhang and Bai, 2010).

Inorganic silica gel systems exist either as aqueous dispersion, called colloidal silica (Iler, 1979; Jurinak and Summerss, 1991; Nasr-El-Din and Taylor, 2005) or solution, called silicate solution (Iler, 1979; Krumrine and Boyce, 1985; Vinot et al., 1989). Although colloidal silica and silicate solution are different in the form, distribution of silica particles in the aqueous phase and stability against gelation, their gelation mechanisms are qualitatively similar (Iler, 1979; Jurinak and Summerss, 1991; Nasr-El-Din and Taylor, 2005). The gelation of silica-based gels is believed to result from particle bonding and aggregation into long chain networks. Gelation occurs when particle aggregation ultimately forms a uniform, 3D network of long bead-like strings of silica particles (Iler, 1979). Sodium silicate is the most popular representative of the silicate solutions.

The gelation time is controllable for both cross-linked polymer and silicate gels, favorable for deep reservoir penetrations. Silicate gel is environmentally friendly (Bauer et al., 2005; Lakatos et al., 2009; Skrettingland and Stavland, 2012); while some of the polymer gel systems contain organic cross-linkers (e.g., phenol) which are harmful to the environment (Nasr-El-Din and Taylor, 2005). The organic cross-linkers are employed to improve the thermal stability and flexibility of the polymer gel systems (Moradi-Araghi et al., 1993). Silicate gel, however, is inherently stable at high temperatures (Bauer et al., 2004; Dai et al., 2010; Lakatos and Lakatos-Szabo, 2012). Silicate solution has water-like viscosity prior to gelation (Skrettingland and Stavland, 2012; Lakatos and Lakatos-Szabo, 2012), allowing it to flow through the water channel with a good injectivity before placement. While the injected gelant of the cross-linked polymers normally behaves as a polymer solution which may leakoff into low permeability zone much more than the injected water, due to its higher viscosity (Liu et al., 2006). The main advantage of the silicate gel is its relative low cost, compared to the other gel systems, including polymer gels (Herring et al., 1984; Vinot et al., 1989; Bauer et al., 2005; Lakatos and Lakatos-Szabo, 2012). More details about silicate gels are presented in section 1.2.

1.1.2. Near wellbore versus in-depth water control treatments

Conformance control techniques may be categorized, based on their treatment location within the reservoir, into three main groups: water shutoff, near wellbore profile control and in-depth profile modifications (Liu et al., 2006).

Water shutoff is referred to those treatments which are performed on the production wells to seal or selectively plug the layers with high water production (Zaitoun et al., 1991; Liang et al., 1993; Seright et al., 1993; Rolfsvåg et al., 1996; Seright et al., 1998; Lane and Seright, 2000; Sydansk

and Southwell, 2000; Eoff et al., 2007). Their objective is to minimize water production, while keeping or increasing oil flow rate (Sorbie and Seright, 1992; Fletcher et al., 1992).

Treatments which are applied to block high permeability layers or fractures around the injection wells are called near wellbore profile control (Jones and Baker 1992; Morganthaler and Schultz, 1994). The objective of these treatments is to divert the injected water to hydrocarbon-bearing strata and less permeable un-swept portions of the formation (Krumrine and Boyce, 1985; Sorbie and Seright, 1992; Fletcher et al., 1992). The injector treatments have some advantages compared to the producer treatments. First, profile control does not require production shut-in. Second, correction of treatment failures is more successful around the injection wells, compared to the production wells. However, the rate of success in water shutoff treatments is higher; hence they are more popular than near wellbore profile control methods (Fletcher et al., 1992).

The third group of conformance control techniques is in-depth water diversion. The objective of this treatment is to place the gel deep into the formation in order to modify the in-depth permeability, hence divert water into un-swept low permeability zone (Fletcher et al., 1992; Bai et al., 2007; Sydansk and southwell, 2000). In-depth treatments are always performed using injection wells, because it is not feasible to inject sufficient fluids into producers to push the treatment chemicals very far into the formation (Krumrine and Boyce, 1985).

Near wellbore treatments can be effective in diverting water to low permeability zone far from the wellbore area, if continuous impermeable barriers separate high permeability watered-out strata from less permeable oil-productive layer, i.e., no cross flow between layers (Seright et al., 2011).

However, in the case of reservoir with cross flow, the injected water will find less flow resistance areas at some distance far from the well and return to high permeability zones or channels (Silva et al., 1971; Krumrine and Boyce, 1985; Seright et al., 2003; Skrettingland and Stavland, 2012). Therefore, to perform an effective water diversion, it is both necessary and desirable to treat as deep as possible into the reservoir (Krumrine and Boyce, 1985). On the other hand, deep placement of treatment, away from the high-pressure gradient zone around the wellbore, will also result in less injectivity impairment, allowing the injection rate to be easily maintained (Fletcher et al., 1992).

However, in-depth treatments are practically much more difficult than near wellbore treatments (Krumrine and Boyce, 1985; Skrettingland and Stavland, 2012). A near wellbore treatment can be obtained either by mechanical isolation of the most productive layers or by low volume chemical treatment. While an in-depth treatment demands injecting large amount of special classes of chemicals, which their gel setting time can be controlled in long distances (Skrettingland and Stavland, 2012). Inorganic silicate gels are deep diverting and cost-effective materials for such a purpose.

1.2. Sodium silicate

Soluble silicates have been the subject of many studies in the last century. Vail (1952) wrote the first comprehensive book on the soluble silicates. Several other books were written later on the subject (Eitel, 1954; Hauser, 1955; Eitel, 1964), which were gathered and reported later by Iler (1955, 1979). ‘Soluble Silicates’ (Falcone, 1982) is the name of book series provided by American Chemical Society (ACS) which reported up-to-date results of silicate studies, including those in the fields of oil and gas reservoirs. A good

review on the history of soluble silicate studies has been presented by Lakatos and Lakatos-Szabo (2012).

The most well-known soluble silicate is sodium silicate (Na-silicate). Na-silicate is a generic name that refers to a family of inorganic compounds which are composed of silica (silicon dioxide) and sodium oxide in various proportions ($(SiO_2)_n$:Na_2O, n<4). The molar ratio between silica and sodium oxide (*n*) plays a major role in the chemical behavior of Na-silicate (Iler, 1979).

Different grades of sodium silicate have been used for several decades in various EOR applications. Traditionally, strong alkaline Na-silicate solutions such as Na-orthosilicate (*n*=0.5) and Na-metasilicate (*n*=1) along with sodium hydroxide (NaOH) were popular for alkaline flooding processes (Campbell, 1977; Krumrine, 1982; Larrondo et al., 1985). Krumrine (1982) summarized some of the advantageous properties of Na-silicate, which are beneficial in EOR applications for enhancing water displacement efficiency: increasing water-wetness of the mineral surfaces, reducing retention of surfactants and alkali consumption, reducing interfacial tension, and so on.

Na-silicate with higher molar ratios (*n*>1.6) shows polymeric properties, and gels under certain conditions, such as low pH, high temperature and so on (Iler, 1979). Silicate gels have been traditionally used as grouting and cementing agents for several decades (Baker, 1982; Krumrine and Boyce, 1985; Bauer et al., 2005). The unique characteristics of Na-silicate gel made it a viable candidate for applications in oil and gas reservoirs (Krumrine and Boyce, 1985; Lakatos and Lakatos-Szabo, 2012).

1.2.1. History of silicate conformance control methods

Na-silicate was first proposed for reservoir profile modifications as a patent by Mills (1922). Later, Kennedy (1936) reported a study on application of some chemicals, including sodium silicate, for water shutoff purposes in production wells. Thirty years later, Robertson and Oefelein (1967) studied and tested silicate gel for plugging thief zones around the injection wells (profile control). Smith et al. (1969) reported laboratory and field studies on silicate gels to plug near wellbore high permeability matrix rock. Their field testing demonstrated that the alkaline silica gels were effective in reducing flow through bypass zones. Na-silicate potentials for conformance control treatments were increasingly being detected in the 70s and 80s by proposing numerous patents (Krumrine and Boyce, 1985). The application of acidic silicate gels for near wellbore water control was addressed by Cole et al. (1978, 1981) and Sparlin and Hagen (1984). The results of a selective gas shut-off treatment using sodium silicate in the Prudhoe Bay field were later reported by Herring et al. (1984).

Krumrine and Boyce (1985) presented an outstanding review paper which addressed silicate gel potentials for profile modification by reviewing literature studies and patents. They also pointed out a list of organic and inorganic agents for Na-silicate gelation. According to Krumrine and Boyce (1985), Na-silicate's viscosity, gelation time, and gel strength depend on various factors such as pH, temperature, salinity, and mechanical shear rate. Later Vinot et al. (1989) performed an experimental study on viscosity, gel time and syneresis of Na-silicate. They addressed some of the main challenges in the field application of Na-silicate: poor understanding of gelation mechanism, lack of effective methods to retard gelation, limited penetration of Na-silicate solutions into the formation due to the buffering capacity of the

rock, and non-durable blockage. They proposed a diester as a gelling agent to retard Na-silicate gelation.

Application of sodium silicate for conformance control treatments became more popular since almost 20 years ago, especially in the Norwegian continental shelf of the North Sea, due to the growing number of depleted reservoirs with high water production in this region. The thermal stability of silicate gel makes it a suitable candidate for treating high temperature oil-fields in the North Sea. Furthermore, silicate gel is one of the few gelling systems which have got environmentally benign approval from Norwegian authorities (PLONOR) for reservoir treatments. Lund and Kristensen and their colleagues (Lund and Kristensen, 1993; Kristensen et al., 1993) performed several experimental studies and field trials to qualify Na-silicate for water shutoff applications in the North Sea. They addressed silicate adsorption on the quartz surface. They also studied the effects of different minerals on buffer capacity of the formation. Lund et al. (1995) and later Rolfsvåg et al. (1996) presented the results of relatively deep water shutoff treatments in oil producers at the Gullfaks field in the North Sea. A numerical simulation method was developed by Rolfsvåg et al. (1996) which matched the observed kinetics of the Na-silicate gelation process. Later, Børeng and Svendsen (1997) reported a water shutoff using silicate gel in the Statfjord field at the North Sea.

Nasr-El-Din et al. (1998) have reported field application of Na-silicate for water shutoff treatments in Saudi Arabia. Nasr-El-Din and Taylor (2005) experimentally evaluated a Na-silicate/urea system for water shutoff treatments which was activated by temperature. Urea was used as an internal activator, which is hydrolyzed at elevated temperatures. Later Al-Dhafeeri et

al. (2008) presented an evaluation on sodium silicate gel to be used in Arab-C carbonate reservoir in Saudi Arabia.

Bauer et al. (2004, 2005) and later Dai et al., (2010) confirmed the thermal stability of Na-silicate gel for application as profile control agent in high temperature reservoirs.

Lakatos and his colleagues have done extensive works on silicate gel and its combination with other chemicals for more than 20 years. They have reported many pilot tests on silicate and silicate/polymer applications for well plugging in Hungarian and Serbian oil fields (Lakatos et al., 1990, 1993, 1998, 1999, 2009). As reported by Burns et al. (2008) and Lakatos et al. (2009) the gel strength of in-situ formed silicate gels is improved by addition of polymers.

Although Na-silicate gel has been widely applied in many successful near wellbore treatments, it is not recognized yet as an in-depth profile modifier, despite its remarkable potentials for such a purpose (Krumrine and Boyce, 1985). However recently, Stavland et al. (2011a, b) and Skrettingland and Stavland (2012) studied Na-silicate gel system for an in-depth water diversion in the Snorre oil field at the North Sea. They first qualified Na-silicate gel using static and sand-pack flooding experiments. The main drawback of their experimental study was quantifying the gel time using an inaccurate visual method by defining gel color codes. The experimental results were then used in designing a pilot test in the Snorre field (Skrettingland and Stavland, 2012). They reported a good agreement between field results and laboratory observations.

1.2.2. Theory of silicate gelation

Monomer silicate in the solution is made up of tetrahedral structures of silicon and oxygen atoms. In each tetrahedron, silicon atom is located at the center of

an oxygen-cornered, four sided pyramid. In Na-silicate, each oxygen atom is typically linked to a sodium or hydrogen atom, or it may be associated with another silica tetrahedron to form dimer. The chemistry of silica is quite complex, so the exact mechanism of silicate gelation is not fully understood (Smith et al., 1969; Vinot et al., 1989). However, there are many studies that attempt to explain the mechanism of silicate gelation (Hurd, 1938; Hurd et al., 1944; Merrill and Spencer, 1950; An-Pang, 1963). Iler (1979) has summarized the available literature and described the chemistry of silicate polymerization in detail.

Silica particles carry negative electrical charges in alkaline, neutral or weakly acid solutions, which retard the gelling by electrostatic repulsion (Hurd, 1938; Vinot et al., 1989). Based on the classical DLVO theory (Hiemenz, 1977), at high pH values (pH > 11) particles repel each other with very strong electrostatic forces. Consequently monomer and dimer species dominate in the solution and silica solution is stable against gelation at high pH. Silicate species aggregate to form higher-order oligomers by addition of acid or surface inorganic salts and alcohol (An-Pang, 1963; Iler, 1979). According to Iler (1979), addition of acid reduces pH of the solution, hence diminish electrostatic forces. Addition of surface inorganic salts and alcohols reduces dielectric constant of the solution and compresses the double layer (charge screening). The silanol groups within the polymers condense to build the individual bigger particles. Polymer chains and eventually gel are formed by aggregation of these particles. Gelation occurs when particle aggregation ultimately forms a uniform, three-dimensional network of silicate particles. When gelation begins, the initially transparent solution of Na-silicate starts to become cloudier. That cloudiness thickens as the gel develops, and the gel’s

appearance is sometimes used as a qualitative measure of gelation time (Stavland et al., 2011a, b).

Based on Hurd's viewpoint (Hurd et al., 1944), which was confirmed later by An-Pang (1963), Iler (1979) and Krumrine and Boyce (1985), when acid material is added to Na-silicate solution, a monosilicic acid is formed which later condenses into long chains of polysilicic acids. Therefore, the effect of different variables, i.e., pH, silicate concentration, temperature and salinity, on the rate of silicate polymerization can be explained by the reactions of silicic acids in the solution.

Effect of pH and silicate content. An-Pang (1963) suggested the following reactions of silicic acid species as the solution pH is reduced by addition of acid:

$$H_2SiO_4^{2-} \xrightarrow{H^+} H_3SiO_4^- \xrightarrow{H^+} H_4SiO_4 \xrightarrow{H^+} H_5SiO_4^+ \qquad (1.1)$$

At high pH, $H_2SiO_4^{2-}$ and $H_3SiO_4^-$ are the dominant ions, which react very slowly, since both have negative charge. The dominant species at a lower pH (slightly alkaline or neutral) are $H_3SiO_4^-$ and H_4SiO_4, so the condensation process starts and may be expressed by the following reaction:

$$H_3SiO_4^- + H_4SiO_4 \rightarrow (OH)_3Si-O-Si(OH)_3 + OH^- \qquad (1.2)$$

Two silanol groups form a new bond in which an oxygen atom bridges the silicon atoms to produce siloxane (Si-O-Si) (Iler, 1979). Based on Eq. (1.2), a hydroxyl ion is liberated as a result of the condensation reaction. This implies that polymerization causes the pH to increase gradually. The resultant dimers polymerize by reacting with $H_3SiO_4^-$ to form trimers in alkaline solutions.

The polymerization process continues and finally forms the alkaline gel network.

At acidic pH values (ranging from 4 to 6), H_4SiO_4 and $H_5SiO_4^+$ react to form a different type of dimer, which finally results in acidic silica gel. The acidic gels are relatively firm, elastic and quite clear, whereas the alkaline gels are softer and opalescent (Smith et al., 1969). Acidic gels have fast gelation, while alkaline silicate gels have longer and controllable setting times (Smith et al., 1969; Krumrine and Boyce, 1985). Therefore, alkaline silicate gels are more suitable for reservoir profile modifications (Krumrine and Boyce, 1985), which is the subject of current study.

Effect of temperature. Jurinak and Summers (1991) suggested that at fixed pH and salinity, the gelation time of silicate as a function of temperature follows Arrhenius equation:

$$t_g = Ae^{E_a/RT} \tag{1.3}$$

where E_a is the activation energy, R is the gas constant, T is the absolute temperature and A is the pre-exponential factor. Assuming a first-order kinetic reaction, A in Eq. (1.3) has the gelation time unit. According to Eq. (1.3), the polymerization rate increases as the temperature rises, hence the gelation time decreases.

Effect of salinity. Addition of salt to an alkaline solution results in charge screening, which decreases gelation time. Divalent metal ions such as Ca^{2+} and Mg^{2+} are more effective in screening the silica particles and consequently accelerate the gelling kinetics more than monovalent cations (Jurinak and Summers, 1991). They also form metal silicate precipitations via ion exchange, which are relatively insoluble in a wide range of pH values. For

example in the case of magnesium chloride, the reaction is as follows (Krumrine and Boyce, 1985):

$$2\,(\equiv SiO^{-}Na^{+}) + MgCl_2 \rightarrow 2\equiv SiO^{-}Mg^{2+} + 2NaCl \qquad (1.4)$$

Syneresis. After gelation time, the gel network continues to reform, causing the gel strength to gradually increase. As the system approaches equilibrium, the gel shrinks and expels the containing liquid (Vinot et al., 1989).The first systematic investigation of such syneresis in silicic acid gels was done by Holmes et al. (1919). Later, Ferguson and Applebey (1930) investigated the kinetics of silicic acid gels. Vinot et al. (1989) also reported a study on the effects of silicate concentration and temperature on Na-silicate shrinkage. Brinker and Scherer (1990) discussed syneresis and the factors affecting it in detail from the literature. They suggested that syneresis is generally attributed to the formation of new bonds (siloxane bonds) during gel development by condensation of two silanol groups (–Si-OH). Gel shrinkage occurs because the formed siloxane bond (see Eq. (1.2)) takes less space than the two individual silanol groups from which it derived. According to Brinker and Scherer (1990), since the same reaction (i.e., condensation) is responsible for both gelation and syneresis, the rates of gelation and syneresis are affected in the same way by different factors. A faster gel time results in an earlier syneresis with higher rate of shrinkage (Ferguson and Applebey, 1930). This was later confirmed by Vinot et al. (1989). They observed that increasing silicate concentration and temperature increase the syneresis. Syneresis is irreversible in most inorganic gels. It is ultimately stopped by the remaining repulsive forces between particles (Brinker and Scherer, 1990)

1.2.3. Considerations for sodium silicate in-depth applications

Reservoir in-depth profile modification is a challenging process, since different reservoir and fluid parameters simultaneously impact the gel kinetics and rheology. Similar to the other polymer treatments, injecting Na-silicate solution into reservoirs is subject to different shear rates, which vary from near wellbore area to the greater distances far from the injector. To our knowledge, the effect of shear rate on Na-silicate gelation has not been addressed in literature.

The concentration and pH of the injected Na-silicate solution change as the solution mixes with the reservoir fluids. The degree of pH change depends on the buffer capacity of the mixed formation water and Na-silicate solution. The pH of the formation water depends on the rock mineralogy (Kristensen et al., 1993). High level of silicate adsorption on the rock surfaces may also affect silicate concentration. Any change in silicate content or pH greatly affects the Na-silicate gelation kinetics (Eq. (1.2)).

Salinity and the types of ions in the formation water are other important factors that affect the Na-silicate gelation kinetics. The possibility of precipitation and unwanted plugging in the presence of divalent ions, mainly Ca^{2+} and Mg^{2+} (Eq. (1.4)), is one of the main challenges in deep application of Na-silicate. Low salinity water pre-flush is practically used to dilute the ions' concentration in the formation.

Reservoir temperature plays an influential role in the gelation kinetics (Eq. (1.3)) and precipitation. Water flooding normally creates a temperature gradient in the reservoir, i.e., cold around the injector and hot deep into the reservoir. This temperature profile can be used as a controlling parameter for Na-silicate gelation.

After determining the desired distance in the formation for water control treatment, it is important to predict the effects of different reservoir factors on

Na-silicate gelation, in order to control the gel placement in the predetermined position. Also, the viscosity of the injected solution has to be kept low enough (ideally water- like) prior to placement, to allow easy injection deep into the formation (Eoff et al., 2007) and to avoid damaging oil-bearing matrix (Seright et al., 2011; Skrettingland and Stavland, 2012). The next step is to ensure that the strength of the formed gel is high enough to withstand the force imposed by the injected water. The factors that affect Na-silicate gel strength have not been quantitatively studied in the literature. Finally it is important to ensure the long term stability of the formed gel. This property is related to the gel shrinkage (syneresis), which may cause the blocked reservoir zone to recover a fraction of its original permeability (Vinot et al., 1989).

2. OBJECTIVES

The main objective of the thesis work is to evaluate alkaline sodium silicate gel system for in-depth reservoir treatments to enhance water sweep efficiency, using experimental and numerical studies.

To achieve this objective, the main factors which affect silicate gel time, strength and shrinkage are addressed. Furthermore, sodium silicate behavior in porous media, including injectivity, preferential flow path, leakoff into the matrix, adsorption/retention, gelation time, gel profile and strength are studied using unconsolidated sand cores. Finally, some of the main considerations in field application of sodium silicate are addressed using numerical simulations.

3. MATERIALS, METHODS AND APPROACHES

In this section, a description of different types of materials and methods used in the experimental works and the applied calculation approaches are presented.

3.1. Materials

3.1.1. Aqueous phase

Na-silicate solution was supplied by BIM Kemi AB, Norway. The Na-silicate content in the solution was 35.7 wt%. The molar ratio (*n*) of the sample was 3.35. The content of silicate and sodium oxide was 27.3 and 8.4 wt%, respectively, as specified by the supplier. This solution had a density of 1.368 g/cm^3 and a pH of about 11.4 at 20 °C. The Na-silicate samples were stored in plastic containers. The pH adjustment was conducted using diluted HCl solution (2 M). To clean the gel from equipments and containers, NaOH solutions were used to dissolve Na-silicate by increasing the solution pH.

Solutions with Na-silicate content between 3 and 6 wt% were prepared by diluting the supplied sample with distilled water (DW). DW was obtained by purifying tap water through Milli-Q Millipore. Other liquids, such as synthetic seawater (SSW), low-salinity water (LSW, volumetric dilution ratio SSW:DW is 1:24) and water containing single cations (Ca^{+2} or Mg^{+2}), were also used. The composition of SSW is given in Table 3.1.

Table 3.1. Chemical composition of synthetic sea water (SSW).

Component	NaCl	Na_2SO_4	$NaHCO_3$	KCl	$MgCl_2$	$CaCl_2$
Concentration (g/l)	23.38	3.41	0.17	0.75	4.24	1.44

3.1.2. Oil phase

Normal decane (*n*-C_{10}) was used as the base oil phase. It was supplied by Chiron AS in HPLC grade (purity >99%). N,N-dimethyldodecylamine (NN-DMDA) was used as an oil soluble additive with the concentration of 0.01 M in *n*-C_{10} to represent natural base in the crude oil (Hamouda and Alipour Tabrizy, 2013). It was supplied by Fulka (purity >99%).

Asphaltene was used to represent the polar and heavy fraction of crude oil in few tests. Asphaltene was prepared by precipitation from crude oil in excess of *n*-heptane (1:40) according to ASTM standard method. The mixture of *n*-heptane and crude oil was shaken for at least twice a day and then left for 48 hours to equilibrate. The mixture solution was then centrifuged and filtered through a 0.22 micrometer filter (Millipore), and dried for 1 day under vacuum at room temperature. The dried asphaltene was then dissolved in toluene. A synthetic oil was prepared with the composition of 50.88 mole% *n*-C_{10}, 0.04 mole% NN-DMDA, 49.02 mole% toluene and 0.06 mole% asphaltene. This synthesized oil was used to study the effect of Na-silicate on the interfacial tension with oil.

3.1.3. Solid phase

Unconsolidated cores were prepared by packing sand particles, with different grain sizes, in the sand-pack tubes. The chemical composition of the used sand particles, supplied by, is given in Table 3.2. Oil Red O and Methylen Blue powders, supplied by Sigma Aldrich were used to dye oil and Na-silicate solution in red and blue colors, respectively. The dyed liquids were used in sand-pack flooding experiments to identify water and gel propagations in porous media.

Table 3.2. Chemical composition of sand particles.

Component	SiO_2	Al_2O_3	Na_2O	K_2O	CaO	TiO_2	Fe_2O_3
Content (wt%)	99.70	0.07	0.03	0.02	0.006	0.001	0.01

3.2. Methods

3.2.1. Evaluation of sodium silicate properties

pH measurements. The Mettler Toledo S20 Seven Easy™ pH meter was used for pH measurement. The pH of a Na-silicate solution increases gradually with time, after adjustment of the pH as predicted by Eq. (1.2). In order to maintain the consistency of the reported data, all the pH measurements were carried out no more than 3 min after preparation of the samples.

Interfacial tension measurement. The oil-water interfacial tension was measured at room temperature by Drop Volume Tensiometer 30 (Kruss DVT30) supplied by KRÜSS GmbH, Germany. The injection rate in all the experiments was within 50-3 µml/min. The oil-water interfacial tension was estimated with built-in software system according to the Eq. (3.1):

$$\sigma = \frac{V_{drop}(\rho_w - \rho_o)g}{\pi D} \tag{3.1}$$

where σ (N/m) is the oil-water interfacial tension, V_{drop} (m^3) is the volume of drop, ρ_w and ρ_o (kg/m^3) are the density of water and oil phases, respectively, g (m/s^2) is the gravity acceleration and D (m) is the diameter of capillary tube.

After each experiment proper cleaning procedure was done, followed by draining all water and oil from the bulk phase glass cylinder and syringe, respectively. The glass cylinder cleaning was followed by rinsing with

isopropanol, DW and finally with next aqueous phase to be measured. Different storage tank was assigned to different fluids to avoid contamination. Finally, at the end of the experiments, the equipment was dismantled, cleaned and dried for next measurements.

Rheological measurements. Viscosity of Na-silicate samples were measured with a Paar Physica UDS 200 Universal Dynamic Spectrometer using rotational module with constant shear rate. Most of the measurements were performed at low shear rate (SR) of 10 s^{-1}, which is close to the average shear rate in the reservoir far from the injection well. The effect of other shear rates, ranging from 1 to 1000 s^{-1}, on gel time was also verified in few experiments. Gelation time (t_g) of a Na-silicate sample was determined based on its viscosity-time profile. t_g was defined as the time after which viscosity deviated from its initial gradual linearity.

Gel strength measurements. Figure 3.1 shows the apparatus that was designed for measuring the gel strength. This tool enabled us to deviate from qualitative methods for assessment of the gel strength such as ringing gel test. The apparatus consists of three main parts: the sample container, the measurement device and the monitoring section.

As shown in Figure 3.1, sample container consists of two concentric cylinders made of polypropylene, to avoid reaction with Na-silicate. The inner radius of the outer cylinder is 16.5 mm and the outer radius of the inner cylinder is 14 mm. So the thickness of the gap between the cylinders is 2.5 mm. The gap is filled with 20 g of Na-silicate sample right after pH adjustment and left to form a gel. To prevent water evaporation before measurement, especially at elevated temperatures, the gap was completely sealed with NBR 70 O-rings 26.64 × 2.62 mm.

To assess the strength of the gel sample at a specified time after gelation, the outer cylinder is fixed in the measurement device. The measurement device is made of two small pulleys with a rope placed in their channels (Figure 3.1). For each measurement, the rope is connected to the top of the inner cylinder of the sample container. Then, the inner cylinder is pulled up vertically by the rope at a constant velocity of 0.5 mm/s. Before the gel breakage, the rope could not move the inner cylinder, since it is fixed by the gel structure. Hence the rope is stretched over time as it is pulling the inner cylinder until the gel sample is broken and the inner cylinder released. The pulley system transfers the internal tension of the rope (F) to an upward force, which is recorded during the test using a weighing balance, connected to a monitoring device.

During each measurement, F increases gradually with time as the rope pulls up the inner cylinder. At the gel breaking point, F experiences a peak value (F_{max}), then it abruptly falls down to a value equal to the weight of the inner cylinder (F_{weight}). The gel strength of a given sample at a certain time after gelation is calculated as

$$gel\ \ strength = \frac{F_{\max} - F_{weight}}{A_{ext}} \tag{3.2}$$

where A_{ext}=0.0045 m^2 is the external area of the inner cylinder. To find the gel strength at various times during the gel formation, several samples with identical properties were prepared and their strength was measured at different times during the gelation process. After each measurement, the gel container with the destroyed gel was disposed and the system was prepared for another measurement.

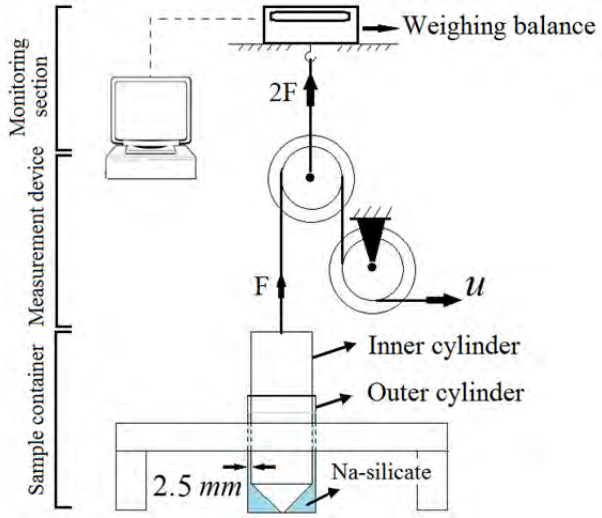

Figure 3.1. Schematic of the constructed gel strength measurement apparatus.

Gel shrinkage measurements. To quantify the gel shrinkage, Na-silicate samples with different initial conditions were kept in completely sealed polypropylene containers for several days. As shrinkage began, the expelled liquid appeared on the surface. The liquid was then removed and weighed as a function of time. Assuming that the initial solution and the expelled liquid had approximately equal densities, the ratio between the weight of the expelled solution and the initial sample (wt% of expelled liquid) provided a measure of the gel shrinkage.

3.2.2. Flooding experiments

Flooding experiments were performed using two types of sand-packs (A and B), which their properties are listed in Table 3.3. The relative permeability end points of the sand-packs are illustrated in Figure 3.2. The endpoints are simply connected with lines, which is a good approximation due to relatively high permeability of the sand-packs. Sand-pack tubes were made of transparent of plexiglass materials, polymethyl methacrylate (PMMA), to

observe Na-silicate gel and fluid profiles. The thickness of the tube wall was 0.9 cm, to tolerate pressures up to 80 bar.

Table 3.3. Physical properties of two types of sand-packs used in dual-permeability flooding.

Property	**Sand-pack A**	**Sand-pack B**
Permeability (d)	12	60
Porosity (%)	43	45
Range of grain size (μm)	90-300	300-500
Irreducible water saturation (s_{wc})	0.31	0.27
Residual oil saturation (s_{or})	0.71	0.75
Length (cm)	78	
Diameter (cm)	1.17	
Total volume (cm^3)	83.80	

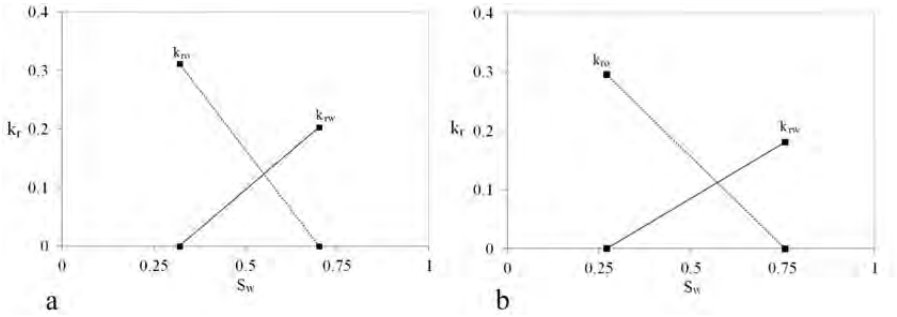

Figure 3.2. Relative permeability (k_r) as function of water saturation (s_w) for sand-packs a) A and b) B.

Dual permeability sand-pack flooding. As shown in Figure 3.3, a parallel configuration of sand-packs A and B is designed to study the performance of Na-silicate in a lab-scale dual-permeability porous medium. Sand-packs were located inside an oven with T=50 ^{o}C. All the fluids, including water, oil and Na-silicate solution, were injected using a syringe pump (Teledyne ISCO Model 260D) with constant flow rate of 0.1 ml/min into transparent Teflon

lines which were connected to the inlet ports of both sand-packs. The effluents of both sand-packs were separately collected in two vials to record oil and water production from each sand-pack. The pressure drop along both sand-packs was separately measured using two accurate digital pressure transducers (E+H model PMD75) and was recorded using Labview™ 2012. Both sand-packs were initially saturated with oil (*n*-C10 and 0.01 M NN-DMDA) and SSW at s_{wc}.

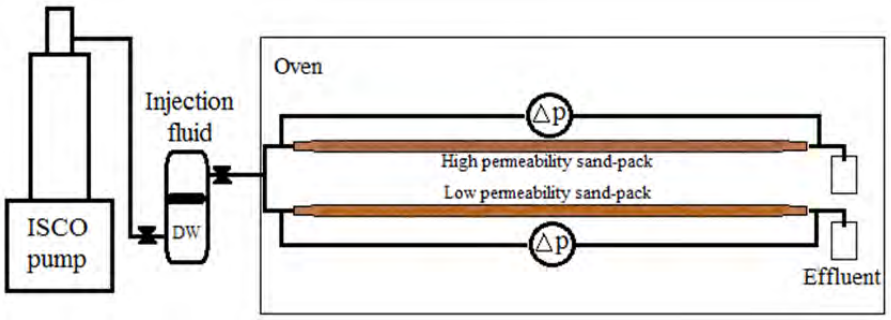

Figure 3.3. Schematic illustration of the experimental set up for dual-permeability sand-pack flooding.

Measurement of silicon dynamic adsorption. To evaluate silicate dynamic adsorption, the effluents of a sand-pack (A) were analyzed for silicon content using ICP (Inductively Coupled Plasma) system. The effluent samples were analyzed by Intertek West Lab AS, Norway. Silicon concentration in the injected fluid was low enough (<100 mg/l) to be within the accuracy range.

3.3. Numerical approaches

3.3.1. Pore-scale modeling of displacements in porous media

Two phase flow in porous media was simulated at pore-scale using the coupled Navier-Stokes and Cahn-Hilliard phase field method (PFM), solved by COMSOL Multiphysics™ with finite element method. Adaptive interfacial

mesh refinement was done to reduce the running time. To enable simulation of non-isothermal phenomena, the equation system was coupled with heat equation. It was assumed that each phase is incompressible and phase change does not occur. The gravity was neglected in all the simulations by assuming 2D horizontal flow. PFM has been described in detail by Wheeler et al. (1995), Jacqmin (1999), Badalassi et al. (2003) and Yue et al. (2004). A brief description of the method is presented in this section.

Phase-field order parameter (ϕ) is defined such that the relative concentration of the two components are $(1+\phi)/2$ and $(1-\phi)/2$. In this definition, $\phi = \pm 1$ represent two components and $-1 < \phi < 1$ represents the interface. Sharp interface takes place at $\phi = 0$. All the fluid physical properties are interpolated between two phases using the relative concentration of the phases:

$$\upsilon(\phi) = \frac{(1+\phi)}{2}\upsilon_1 + \frac{(1-\phi)}{2}\upsilon_2 \tag{3.3}$$

where υ denotes each property, including density (ρ), viscosity (μ), specific heat capacity (C_p) and thermal conductivity (κ).The moving interface is captured by coupling phase field and modified Navier-Stokes equations, which includes a phase field-dependent surface force. The main governing equations of Cahn-Hilliard phase field coupled with Navier-Stokes and heat transfer (including conductive and convective heat transfers) are presented here. The equation system is given as follows:

$$\frac{\partial \phi}{\partial t} + u.\nabla\phi = \gamma\nabla^2 G \tag{3.4}$$

$$\rho\frac{\partial u}{\partial t} + \rho u.\nabla u = -\nabla p + \nabla.\left[\mu(\nabla u + \nabla u^T)\right] + G\nabla\phi \tag{3.5}$$

$$\nabla . u = 0 \tag{3.6}$$

$$\rho C_p \frac{\partial T}{\partial t} + \rho C_p u . \nabla T = \nabla . (k \nabla T) \tag{3.7}$$

where u is the fluid velocity field, γ is the diffusion coefficient called mobility, G is the chemical potential of the system, p is the pressure and T is the temperature. Mobility is expressed as $\gamma = \gamma_c \varepsilon^2$, where γ_c is the characteristic mobility that governs the temporal stability of diffusive transport and ε is a capillary width that scales with the interfacial thickness. The chemical potential is derived from total energy equation as $G = \lambda \left[-\nabla^2 \phi + \phi(\phi^2 - 1)/\varepsilon^2 \right]$, where λ is the mixing energy density. Phase field considers surface tension as an intrinsic property corresponding to the excess free energy density of the interfacial region (Qin and Bhadeshia, 2010). In the case of a planar interface, surface tension coefficient is obtained by $\sigma = (\sqrt{8}/3)\lambda/\varepsilon$.

Eqs. (3.4) to (3.7) form the governing system of equations for modeling non-isothermal two-phase flow problems. The coupled equation system is numerically solved using proven finite element method performed by the commercial software of COMSOL Multiphysics™ (COMSOL Multiphysics User's Guide, 2011). For discretization by second-order finite elements, the fourth-order Cahn-Hilliard equation (Eq. (3.4)) is decomposed into two second-order equations (Yue et al., 2006) using an auxiliary parameter (ψ):

$$\frac{\partial \phi}{\partial t} + u . \nabla \phi = \frac{\gamma \lambda}{\varepsilon^2} \Delta \psi \tag{3.8}$$

$$\psi = -\varepsilon^2 \Delta \phi + \phi(\phi^2 - 1) \tag{3.9}$$

So the computations are done using five dependent variables of { u , p , ϕ , ψ , T }. The governing equations are supplemented by standard boundary conditions (e.g., inlet, outlet, no-slip, wetted wall and symmetry), which are specified for each model in the related sections. The details about the boundary equations can be found elsewhere (Yue et al., 2006; Zhou et al., 2010). On the solid wetted grains, the following boundary conditions are used:

$$u = 0 \tag{3.10}$$

$$n.\varepsilon^2 \nabla\phi = \varepsilon^2 \cos(\theta_c)|\nabla\phi| \tag{3.11}$$

$$n.\frac{\gamma\lambda}{\varepsilon^2}\Delta\psi = 0 \tag{3.12}$$

where n is the unit normal to the wall and θ_c is the contact angle. Triangular mesh elements are used in all the computations in this work. Time steps sizes are controlled by the numerical solver during the computations, using backward differentiation formula (BDF).

To avoid numerical distortions, interface must be thin enough to approach a sharp interface. A sharp transition minimizes smearing of physical properties as well as better conservation of the area bounded by the zero contour. The interface layer, however, must be resolved by fine mesh. These conditions are described in detail by Zhou et al. (2010) as model convergence and mesh convergence, respectively. Mobility (γ) is another important parameter that affects the accuracy of the PFM (Jacqmin, 1999). γ has to be large enough to retain a more or less constant interfacial thickness and small enough to keep the convective motion (Yue et al., 2006). Different sensitivity studies have been reported by Akhlaghi Amiri and Hamouda (2013) on model convergence, mesh convergence and mobility in modeling two phase flow

through porous media using PFM. Considering the average grain diameter in porous medium as the characteristic length (l_c) and defining Cahn number as $Cn = \varepsilon / l_c$, it was demonstrated that at Cn=0.03 and mesh size $h = 0.8\varepsilon$, the model convergence and mesh convergence are satisfied for phase filed method. Simulations with $\gamma_c = 1$ showed less volume shrinkage and more physically realistic results (Akhlaghi Amiri and Hamouda, 2013).

To achieve numerical accuracy at a reasonable computational cost, it is efficient to have a mesh with dense grids covering the interfacial region and coarser grids in the bulk. In this scheme, refined grids cover the interfacial region and as the interface moves out of the fine mesh, the mesh in front is refined while that left behind is coarsened. Such adaptive meshing is achieved here using adaptive mesh refinement (AMR) technique. The detailed description of AMR can be found elsewhere (Rannacher, 1996; Verfürth, 1996; Verfürth, 1998; COMSOL Multiphysics User's Guide, 2011). AMR is based on an error indicator function, which is the L^2 norm of gradient of a dependent variable. To localize the mesh refinement on the fluid interface, the gradient of order parameter ($\nabla\phi$) is used by the adaptive solver algorithm as the error indicator function as follows:

$$\|e\| = \sqrt{(\frac{\partial \phi}{\partial x})^2 + (\frac{\partial \phi}{\partial y})^2} \tag{3.13}$$

3.3.2. Simulation of sodium silicate behavior in unconsolidated cores

The unconsolidated core flooding experiments were simulated using STARS™, an application of CMG (Computer Modelling Group). The relative permeabilities, silicate adsorption and Na-silicate viscosity increase due to gelation were incorporated in the simulation method.

Two-dimensional (2D) models of sand-packs were built to simulate the processes. It was assumed that permeability and porosity are uniformly distributed in the sand-pack models. The simulated sand-packs were discretized using 5 grids in J direction, and 1 grid in K direction. A sensitivity study was performed on the grid block sizes in I direction, which is the main direction of flow, to find the numerical dispersion impact on the flow profile. The simulation results were compared with the experimental result obtained from flooding sand-pack with non-adsorbing tracer (Cl^-). When the grid size in the I direction is smaller than $L/312$ - where L is the length of the sand-pack- the simulation results showed good agreement with the experimental results.

A new method was developed for simulation of Na-silicate gelation at lab-scale, based on the viscosity increase. The procedure of the method is briefly described as follows. During the simulation process, water, Na-silicate, acid, gel and dead oil were treated as five components. The former four components were considered as the water phase, while the latter one was regarded as the oil phase. Na-silicate component had the physical properties of supplied sample. The concentration of each component at each grid was calculated from the conservation equations for all components. An adsorption term was used in the conservation equation for Na-silicate component.

Prior to injection of Na-silicate and acid, their concentrations and the gel amount in all grids are set to be zero. As Na-silicate and acid are injected, their concentration will gradually increase at each grid and a higher concentration exists at the upstream grids. A simplified reaction scheme for gel formation may be modeled by assuming that the reaction is of the form: water (C_w) + Na-silicate ($C_{Na\text{-}s}$) + acid (C_{Hcl}) $\rightarrow$ gel (C_{gel}), where C refers to the mass fractions of each component in the water phase. In order to simulate

water phase viscosity increase due to Na-silicate gelation, a low value was assigned for the rate of the defined reaction before gelation time while this value was modified to a higher value for the times after gel setting point. The viscosity of the water phase was defined as

$$\mu_w = C_{gel}\mu_{gel} \tag{3.14}$$

where μ_{gel} is the ultimate gel viscosity when the gel is fully formed. According to Eq. (3.14), water phase viscosity increases as a function of produced gel mass fraction. Before gel time, the reaction rate is low; hence the gradient of viscosity increase is low. At gel time water phase viscosity sharply increases to higher values.

3.3.3. Field-scale study of in-depth profile modification

A 2D reservoir model, containing two parallel layers, was used to investigate several sensitivities on application of gel treatment. Table 3.4 gives the reservoir and fluid characteristics used in the simulations.

Reservoir models are simulated using CMG (Computer Modelling Group) simulator. The reservoir length and thickness are L=1000 ft [305 m] and H=90 ft [27.5 m], respectively. It contains two distinct permeability regions, a high permeability (HP) layer with the thickness of h and a low permeability (LP) layer with the thickness of $H–h$. There is one injection well and one production well located at the two ends of the simulated model (x=0 and x=L, respectively), injecting and producing through the entire reservoir thickness. The relative permeabilities for the two reservoir regions are shown in Figure 3.4. A linear saturation dependence relative permeability is assumed for the high permeability streak. Reservoir initial temperature is T=120 ^{o}C, which is flooded by cold water (at 18 ^{o}C).

In all the calculations, the reservoir is represented by 100 grid blocks in I-direction and 30 grid blocks in K-direction. Calculations on a finer mesh did not show considerable increase of accuracy in the results.

To study the propagation of the injected gelling material prior to an in-depth placement, an aqueous phase is defined, called pre-gel Na-silicate, with the physical properties listed in Table 3.4. Pre-gel Na-silicate solution has initial water-like viscosity; however upon pH adjustment, the viscosity increases gradually with a linear trend up to about 8 cp, when the gelation starts (gel setting time). This viscosity increase will affect the propagation of the injected solution slug during in-depth placement and may cause deviation from the water path and penetration into the matrix. So in the numerical simulation, the viscosity of the injected pre-gel solution is set to 4 cp, which is the average viscosity of Na-silicate before gel time. This value also corresponds to the average viscosity of other gelling materials (Seright et al., 2011).

Some numerical experiments were done to compare near wellbore and in-depth gel treatments. Gel treatments were simulated by permeability modifications in a certain length of the HP layer. The permeability reduction due to the gel treatments was simulated by defining a residual resistance factor (F_{rr}), which is the ratio between the original permeability to the reduced permeability of the treated zone. It is assumed that the gel placement is instantaneous and the gel strength remains constant after treatment until the end of simulation time.

Table 3.4. Simulated reservoir fluid properties and computational parameters.

Reservoir properties		**Fluid properties**	
Reservoir dimensions, ft		*Fluid viscosities, μ ,cp*	
Length, L	1000	Water (μ_w)	1
Width, W	30	Oil (μ_o)	1-10
Thickness, H	90	*Fluid densities, ρ, lbm/ft^3*	
Grid definition		Water (ρ_w)	62.4
NX	100	Oil (ρ_o)	44
NY	1	Na-silicate solution	70
NZ	30	*Residual saturations*	
Horizontal permeability, k_h, md		s_{wc}	0.25
LP layer	50	s_{or}	0.22
HP layer	250-50000	*Compressibility*	
Vertical permeability,		All fluids are considered incompressible	
k_v/k_h	0.001-1	*Thermal conductivity, κ, Btu/ftdayF*	
Porosity	0.25	κ_w	8.6
Initial Pressure, P, psi	2000	κ_o	2
Initial Temperature, T,F(^oC)		*Oil in place, ft^3*	
T	250 (120)	Total OOIP	675,000
Rock heat capacity, C_p, Btu/ft^{3}F		Movable OOIP	357,750
C_{prock}	35		
Thermal conductivity, κ, B*tu/ftdayF*			
κ_{rock}	30		

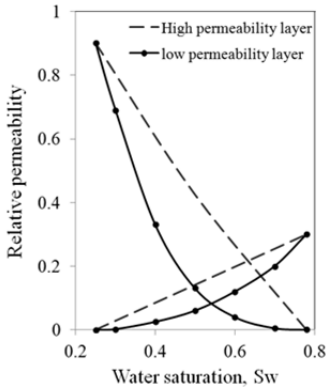

Figure 3.4. Relative permeability curves for low and high permeability media in two-layered reservoir.

4. RESULTS AND DISCUSSION

The main results are summarized and discussed in this section to address the main project objectives. Detailed results and discussion are presented in the enclosed papers.

4.1. Displacement instabilities in porous media

Displacement instabilities, i.e., fingering and channeling, are the major causes of poor sweep efficiency and excessive water production in water-flooded oil reservoirs. The main parameters which cause such instabilities are permeability and viscosity contrasts. These parameters are addressed here along with other factors at pore and field scales.

4.1.1. Pore-level study on the effects of viscosity and permeability contrasts

Pore-scale simulation of fluid flow through porous media demands a method that can handle complex pore geometries and topological changes. The interface capturing approaches, namely level set method (LSM) and phase field method (PFM), are becoming increasingly popular because of their ability to model flow problems with complex topologies using detailed interface calculations. LSM and PFM were compared to assess their performances to capture the physics of two phase flow and respective simulation time.

Two-phase flow with viscosity contrast in homogenous and dual-permeability media were simulated using LSM and PFM (Akhlaghi Amiri and Hamouda, 2013). It was concluded that both methods are able to capture the basic transport phenomena related to viscosity and permeability contrasts, including water fingering and channeling; however PFM was demonstrated to capture

the physical phenomena in more details, i.e. interface stabilities and interfacial tension, especially in heterogeneous porous media. LSM was unsuccessful in capturing volume conservation and simulating stable no-slip boundary conditions. In addition, the running times were considerably less in the case of PFM in simulating different scenarios. This was due to the ease of convergence in the solutions and hence smaller number of time steps. PFM was therefore selected for the performed studies on modelling water-oil displacement instabilities in porous media. PFM equations and simulation using COMSOL were described in section 3.3.1.

The effect of viscosity contrast in water-oil displacement was addressed using a uniform porous medium with the dimension of $0.015 \times 0.009 m^2$, in which the grains were represented by equilateral triangular array of circles. The bulk grain diameter (D_g) and pore throat diameter (D_t) were set as 0.001 *m* and 0.00015 *m*, respectively. To accelerate the process, the homogeneity of the medium was slightly disturbed by enlarging the diameter of ten randomly distributed grains by 10%. The porosity of the medium was approximately 35%. The grain surfaces were defined as wetted walls, having a certain contact angle (θ_c).Water was injected with constant velocity (u_{inj}) at the left hand side inlets of the medium with symmetry boundary conditions on the lateral sides. The pressure was assumed to be zero at the outlets on the right hand side of the medium.

In such a 2D homogenous medium, the forces of the injected water and the fluid properties determine the types of instabilities. Water-oil viscosity contrast in the medium was quantified by the viscosity ratio $M = \mu_w / \mu_o$, where μ_w is the water viscosity and μ_o is the oil viscosity. Capillary number was

defined as $Ca = \mu_w u_{inj} / \sigma$, where σ is the water-oil interfacial tension. *Ca* indicates the relative effects of viscous to capillary forces.

Fluid distributions at water breakthrough time for a range of log *M* and log *Ca* are shown in Figure 4.1. In this study $\sigma = 0.04$ *N/m* and $\theta_c = \pi/2$ (intermediate wetting condition). Blue and red colors represent water and oil phases, respectively and the color gradient represents the interface zone. The combined effect of log *Ca*=-2.6 and log *M*=0 exhibit a stable displacement pattern and other combinations of log *Ca* and log *M* show instability patterns (fingering). Two types of fingering are identified, viscous fingering and capillary fingering. Viscous fingering is mostly evident at lower *M* values with multiple loosely connected or disconnected flow paths. While capillary fingering occurs at lower *Ca* values, when *M* is relatively high. It is characterized by thick interconnected flow paths with an average width of more than 3 pore bodies. In general by keeping constant *M*, sweep efficiency increases with *Ca*, as a result of the dominance of viscous forces. On the other hand by keeping constant *Ca*, sweep efficiency first decreases as log *M* goes from -2 to -1, then increases with log *M*, may be due to transition of flow from viscous to capillary dominant .

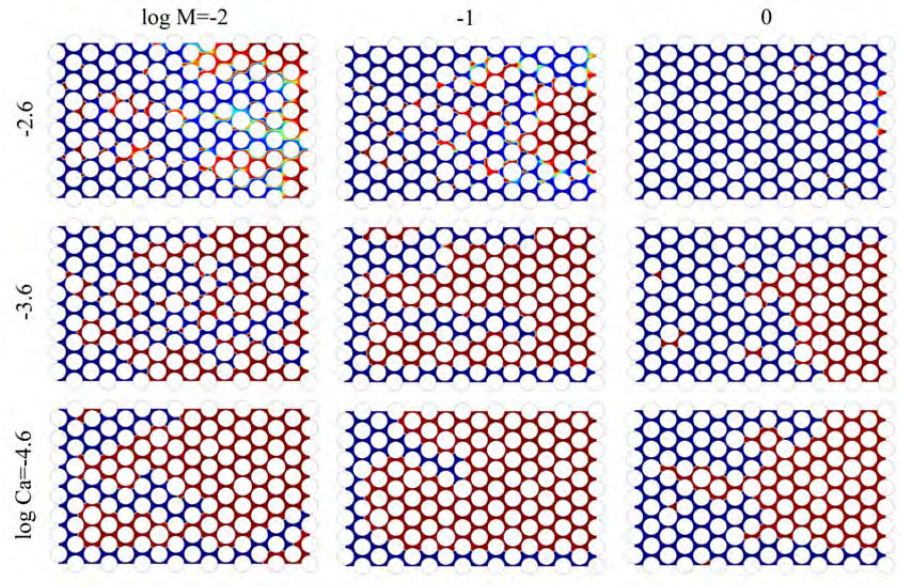

Figure 4.1. Snapshots of fluid distributions at breakthrough times for different fluid displacements with log *Ca*=-4.6, -3.6 and -2.6 and log *M*=-2, -1 and 0.

Three identified displacement regimes can be mapped on a log *M*-log *Ca* stability phase diagram for the conducted numerical experiments (Figure 4.2). The regimes are distinguished by thick boundary zones, as shown in Figure 4.2 with a lighter color, to account for possible errors due to the studied small porous medium. The boundaries of stable displacement are located at log $M \approx 0$ and log $Ca \approx -2.6$. log $M \approx -1$ is considered as the boundary for viscous fingering region and log $Ca \approx -4.6$ is considered as the boundary for capillary fingering region. The shape of the three regions is discussed in detail by Lenormand et al. (1988). Figure 4.2 also demonstrates the boundaries which were obtained by Zhang et al. (2011) using micro-model experimental studies, shown by dashed blue lines. There is a good agreement between the regions' boundaries empirically obtained by Zhang et al. (2011) and those obtained in this work.

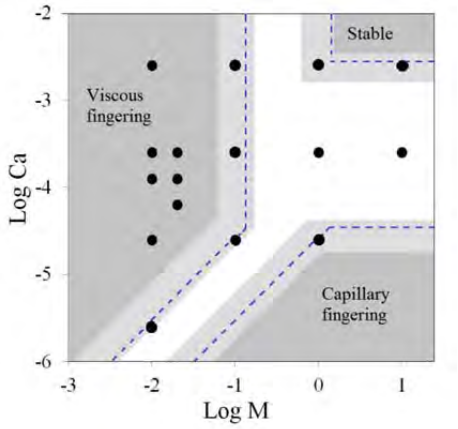

Figure 4.2. log *Ca*-log *M* stability phase diagram showing three regions (dark gray) and the locations of different performed numerical experiments (dots). The boundaries are specified as thick layers (light gray). The boundaries determined by Zhang et al. (2011) are shown as dashed lines.

In a pore-level study, it is realized that there is another parameter which may control the forms of the displacement instabilities by modification of the interfacial shapes in contact with the grain surfaces. This parameter is wettability, which is normally quantified by contact angle. Figure 4.3 shows the fluid distributions for displacement with log *Ca*=-3.9 and log *M*=-1.7 after stabilization at different θ_c values of $\pi/8$, $\pi/2$ and $7\pi/8$, corresponding to strongly water wet, intermediate wet and strongly oil wet conditions, respectively. In general, the water fingers become thinner as the medium becomes less water wet. When the medium is water wet, $\theta_c = \pi/8$, the water phase propagates with three continuous thick fingers with average thickness of 2-3 pore bodies. Two lateral fingers breakthrough, while the middle one becomes stagnant after water breakthrough time. However as shown in Figure 4.3 for the oil wet media, water is split into numerous thin water fingers with average thicknesses less than a pore body. Numerous trapped water volumes are formed in different parts of the oil wet medium with different sizes which

range from several pore bodies to less than a pore body (small water blobs). Water saturation is below 0.5 when medium is oil wet, while it increases more than 30% as the medium becomes strongly water wet. It is worth mentioning that, in general, the water breakthrough happens at an earlier time as the medium becomes less water wet.

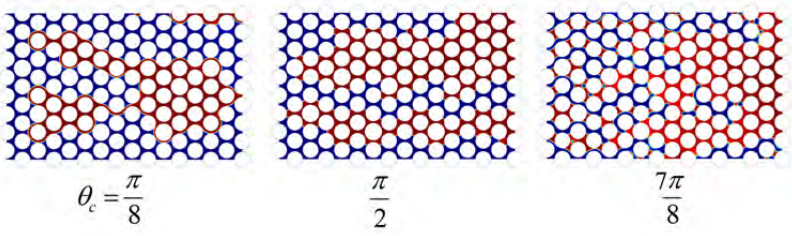

Figure 4.3. Snapshots of fluid distributions at water breakthrough times for the tested case of log *Ca*=-3.9, log *M*=-1.7 with different grain contact angles of $\pi/8$, $\pi/2$ and $7\pi/8$.

Different pore-scale mechanisms are observed in water wet and oil wet conditions which affect the efficiency of the displacements. Figure 4.4 demonstrates four instants in enlarged sections of the medium during water invasion in strongly water wet and strongly oil wet conditions. These mechanisms occur around a gray color marked grain for $\theta_c=\pi/8$. At instant (a), as water front approaches the marked grain, the film of non-wetting oil phase on the surface of the marked grain narrows until it ruptures; so that the water phase just contacts the grain surface. Upon formation of a water-oil-grain contact line, it moves on the grain surface, instants (b) and (c), until water phase surrounds the grain, instant (d). This sequence repeats for all the water invaded grains. Another mechanism in strongly water wet systems is formation of oil blobs as a result of water film bridging in pore throats, instants (a) and (b) above the marked grain. The trapped oil drop is initially

attached to the surrounded grain walls in the pore body, instant (b), which is detached later from the grain walls, instant (c), due to viscous forces.

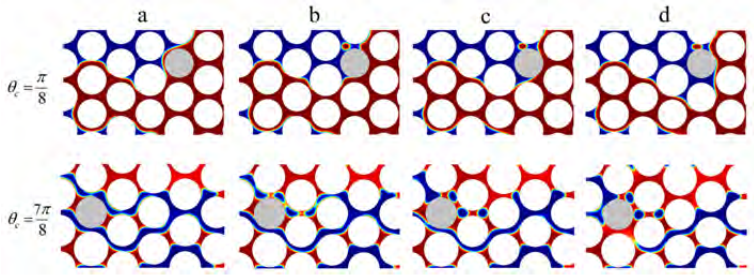

Figure 4.4. Snapshots of fluid distributions in an enlarged section of the medium at four successive instants of a, b, c and d for strongly water wet ($\theta_c = \pi/8$) and strongly oil wet ($\theta_c = 7\pi/8$) conditions in tested case of log *Ca*=-3.9, log *M*=-1.7.

As shown in Figure 4.4 for the strongly oil wet media, the water finger above the marked grain narrows in the throat channels due to growth of oil films around the grains, instant (a), and splits into several parts due to oil film bridging in pore throats, instant (b). This water finger splitting results in forming three small water drops trapped in pore bodies, instant (c). Another water finger splitting phenomenon happens below the marked grain at instant (d) without forming any water blob. Water splitting and trapping reduce the efficiency of oil displacements in oil wet media.

To study the effect of permeability contrast on the displacement efficiency, a dual-permeability medium with a dimension of $0.03\times0.0045 m^2$ is simulated. The grain diameter (D_g) and the pore throat diameter (D_t) in the low permeability area (matrix) are 0.001 *m* and 0.00015 *m*, respectively. The high permeability layer is simulated by decreasing the grain diameter by 20% in one side of the medium. The thickness of high permeability layer is 0.0017*m*. The permeability ratio between the high permeability layer and the matrix is

approximately 10. The water-oil contact angle on the grain surfaces is set to the intermediate wetting condition, $\theta_c = \pi/2$. A Symmetric boundary condition is imposed on the high permeability lateral side, to extend the geometry in this direction. The low permeability lateral side has no-slip boundary condition. Water phase is injected from the left hand side of the domain at a constant flow velocity (u_{inj}). The pressure is assumed to be zero at the outlets on the right hand side of the medium.

Figure 4.5 shows a sensitivity study done for displacement at log *Ca*=-3.6 and log *M*=-1 to 1. As shown in Figure 4.5a, water channeling through high permeability layer is the common phenomenon in all the performed numerical experiments. However the displacement profiles are dependent on *M*. The water channel thickness in the high permeability layer (Figure 4.5a) and the water sweep efficiency (Figure 4.5b) both increase with log *M*. At log *M*=-1, water forms the thinnest possible channel through the high permeability layer toward the outlet. As log *M* increases to 0, the thickness of water channel up to the middle of the medium increases and few more pore bodies in the matrix are swept, close to the inlet. As log *M* increases to 1, the displacement becomes more stable, however water can displace almost half of the matrix oil (s_w < 0.8). As a conclusion, Figure 4.5 reveals that water channeling may be serious even when the displacing phase is more viscous than the displaced phase (log *M* > 0) and it is exacerbated as *M* decreases.

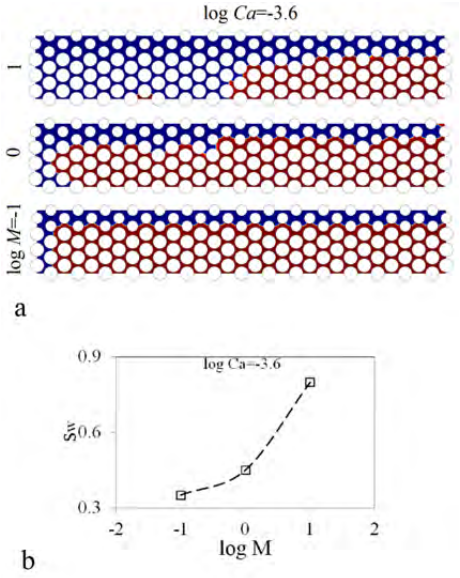

Figure 4.5. Water-oil displacement results in dual-permeability model with log *Ca*=-3.6 and different log *M* : a) snapshots of fluid distribution at water breakthrough time, b) s_w versus log *M*.

Water channeling phenomenon frequently happens in most of the water-flooded oil fields, since high permeability streaks and adjacent layers with permeability contrast are prevalent geological structures. In addition to the viscosity ratio which shown to affect water channeling at pore-scale (Figure 4.5), there are different other parameters which control the form and the intensity of this phenomenon at larger scales. Therefore a field-scale study which addresses water channeling and the main effective reservoir parameters can be useful to provide a better understanding of the problem.

4.1.2. Field-scale study of water channeling effect

Water-oil displacement in a two-layered reservoir with permeability contrast is addressed in this section. The reservoir and fluid properties of the simulated reservoir model as well as the numerical scheme were presented in section

3.3.3. Different sensitivity studies are done to evaluate the factors which influence water channeling phenomenon, including permeability ratio between the high permeability (HP) and the low permeability (LP) layers, HP layer thickness, the ratio between vertical and horizontal permeabilities (k_v/k_h), cross flow between layers, the relative position of the HP and the LP layers and the injection flow rate. In all the numerical experiments in this study viscosity ratio is 1.

One of the main reservoir characteristics which highly affect fluid displacements in a layered medium is permeability contrast between layers. Figure 4.6 shows the water-flooding oil recovery factor (RF) and water cut% as functions of the injected water pore volume (PV) for various permeability ratios, ranging from 5 to 100. In this test, the relative thickness of HP layer to reservoir thickness is h/H=0.2, k_v/k_h=0.01 and cross flow occurs between layers. A higher permeability ratio results in an earlier primary water breakthrough from the HP layer (indicated by the deviation point from linearity in RF profile or first jump in the water cut profile). The difference in the primary breakthrough times becomes very small at high permeability ratios, so that primary breakthrough time does not change as permeability ratio increases from 100 to 1000. As permeability ratio increases, the secondary water breakthrough in LP layer (indicated by RF plateau or second jump in water cut profile) occurs at a later time. At higher permeability ratios, the first jump in water cut is greater (Figure 4.6b) which indicates that a larger proportion of the injected water flows through water channel at higher permeability ratios. While the second jump in water cut profile is greater for the reservoirs with lower permeability ratios, since water sweep efficiency in LP layer is higher at lower permeability ratios. Ultimate oil recovery factor

and water cut are therefore higher at lower permeability ratios, as shown in Figure 4.6a and b.

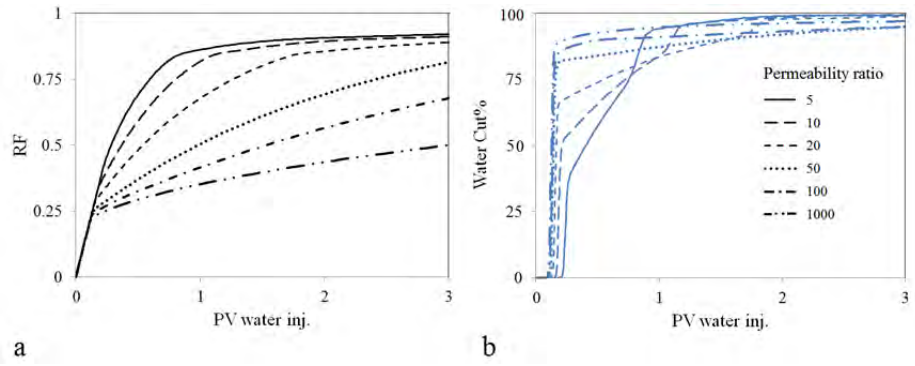

Figure 4.6. The effect of permeability ratio between the layers in the two-layered reservoir model on: a) oil recovery factor and b) water cut as functions of the injected water PV.

Figure 4.7 compares RF in the layered reservoir with different h/H. In the studied case, the permeability ratio is 20, k_v/k_h=0.01 and cross flow occurs between the layers. As h/H increases, primary water breakthrough happens in a later time due to the larger volume of the HP layer, which takes more time to be swept. However, the secondary water breakthrough time is shorter and ultimate oil recovery is higher for the smaller h/H, as shown in Figure 4.7.

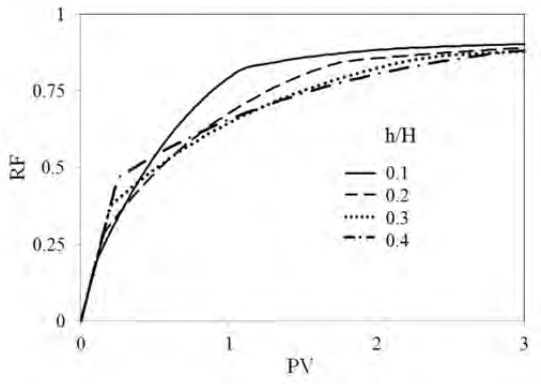

Figure 4.7. The effect of the HP layer over reservoir thicknesses (*h/H*) on oil recovery factor as a function of water injected PV.

The effect of cross flow on RF and water cut is shown in Figure 4.8. In the simulated model, permeability ratio is 20, h/H=0.2 and k_v/k_h=0.01. Figure 4.8 shows that RF and water cut for the studied cases (with and without cross flow) are different just in the time period between water breakthrough times from the HP and the LP layers. During this time period RF is almost linear and lower in the reservoir without cross flow, compared to the other case. Water cut for the reservoir with cross flow gradually increases after the first breakthrough time until the second one. While in the other case water cut almost stabilizes after the first water breakthrough, then increases at the second breakthrough. As depicted in Figure 4.9, in the reservoir with cross flow, due to the flow communication between the layers, the formed water channel expands to the LP layer, thicker around the water front in the LP layer, and thinner near the producer. So after the primary water breakthrough time, as water front in the LP layer moves toward the producer, the thickness of the broken through water channel increases, hence water cut increases. While in the case without cross flow, there is no flow contribution from the HP layer to the LP layer; hence RF is linear and water cut remains constant between the two breakthrough times.

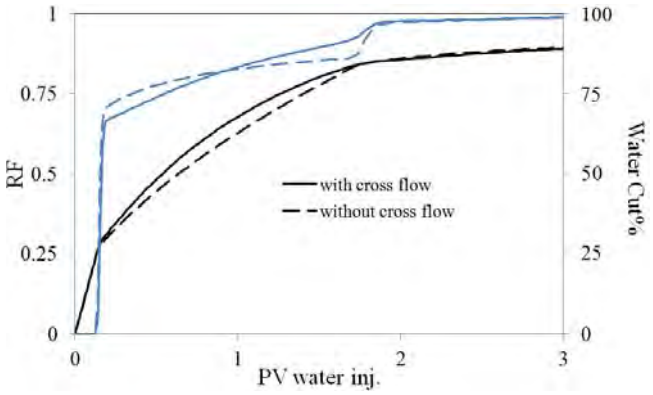

Figure 4.8. The effect of cross flow between layers on oil recovery factor and water cut% as functions of water injected PV.

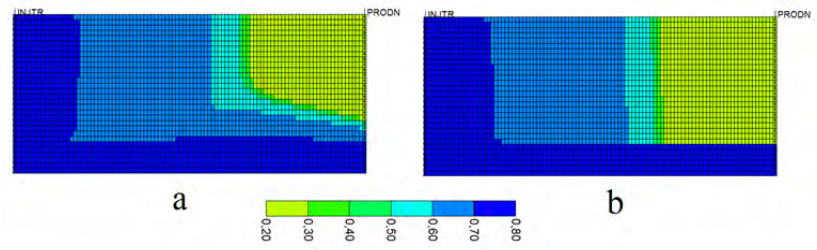

Figure 4.9. Snapshot of water saturation profile after 1 PV injection of water in the layered reservoir a) with and b) without cross flow.

Figure 4.10 shows RF and water cut profiles as functions of the injected water PV for the different values k_v/k_h, ranging from 0.001 to 1. The study is performed on a model with permeability ratio of 20, h/H=0.2 and with free cross flow between the layers. Similar to the cross flow effect, vertical permeability mainly affects RF between the primary and the secondary breakthrough times. Higher vertical permeability results in a higher RF in this time period. However, when vertical and horizontal permeabilities are equal, which is rarely occurred in the real cases, ultimate recovery also increases, compared to the lower values of the vertical permeabilities. As shown in Figure 4.11, for the reservoir with k_v/k_h=1, water channel through the HP layer strongly contributes water sweep efficiency in the LP zone, so that the maximum water saturation level (s_w=0.78) goes up from the HP layer almost to the middle of the LP layer. However, as k_v/k_h decreases to 0.1, the contribution of the HP layer decreases, so that just a thin layer with s_w=0.78 is formed above the HP layer.

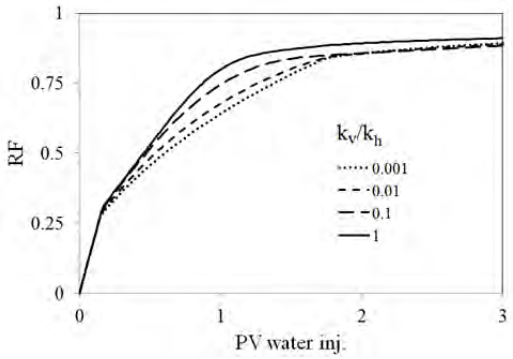

Figure 4.10. The effect of k_v/k_h on oil recovery factor as a function of water injected PV.

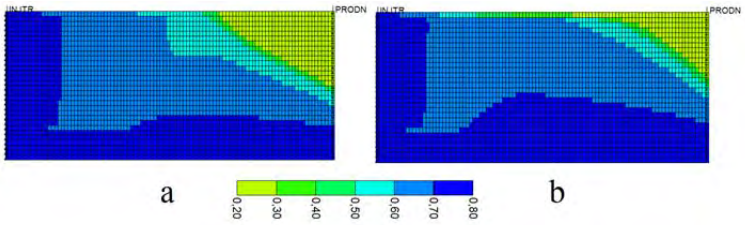

Figure 4.11. Snapshot of water saturation profile after 1 PV injection of water in layered reservoir in which k_v/k_h is set to a) 0.1 and b) 1.

The effects of the capillary forces are negligible at field-scale studies. So the resultant fluid profiles are due to the cooperation of the viscous forces and the gravity. Viscous forces are directly affected by the injection rate (pressure gradient in the reservoir). Figure 4.12 illustrates RF versus the injected water PV for different injection rates, where HP layer is located below the LP layer (black trends) or above (green trends). The study is performed on a model with h/H=0.2, permeability ratio of 20 and with cross flow between layers. In general, the reservoir models with the HP layer at the top have higher oil recovery factor than those with the HP layer at the bottom. It can be seen that when the HP layer is at the bottom, RF increases as the injection rate increases (higher viscous forces); however it is vice versa for the case with the HP layer at the top, i.e., RF increases as the injection rate decrease. This happens since

gravity forces are dominant at low injection rates when HP layer is at the top. Gravity forces result in water in the water channel to penetrate into the LP layer, especially at lower injection rates, and sweep some of the oil in the matrix.

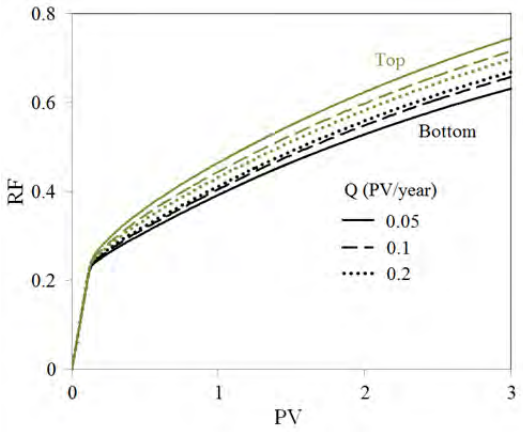

Figure 4.12. The effect of water injection rate and the HP layer position on oil recovery factor as a function of water injected PV. Black and green trends are for the case with the HP layer at the bottom and top, respectively.

Based on the numerical experiments done in this section, it is concluded that the layered reservoirs, especially those with high permeability contrast, often need improved sweep after water breakthrough to diminish water production and to recover the remaining oil. To enhance water sweep efficiency in such reservoirs, it is necessary to divert the water from high permeability to the matrix. This can be done by increasing flow resistance in the water channel using gel treatment.

Next section compares the performance and the main considerations for the near wellbore and the in-depth conformance control methods applied in the two-layered reservoir to reduce water cut and enhance oil recovery. The outcome of this section can help better selection of the treatment method, based on the reservoir characteristics.

4.1.3. Near wellbore versus in-depth gel treatments

A two-layered reservoir model, similar to what was described in section 4.1.2, is studied in this section. In this model the permeability ratio between the layers is 100, h/H=0.2, k_v/k_h=0.01 for the two layers and viscosity ratio is 1. More details about the reservoir and fluid properties were presented in section 3.3.3 (Table 3.4).

Gel treatments were simulated by permeability modifications in the HP layer close to the injector for the near wellbore and at the middle of the reservoir (x=500 ft) for the in-depth treatments. The residual resistance factor (F_{rr}) in the treated zone was increased to 25. It was assumed that the gel treatments affect the total thickness of the HP layer in the treated area. The length of the treated zone was 100 ft (0.1L) for the both treatments. It was also assumed that the gel placement is instantaneous (at 1.5 PV) and its strength is permanent.

Figure 4.13 shows the results of water flooding after 1.5 PV water injection (before gel treatment). Due to a high permeability contrast between the layers, most of the injected water flows through the water channel. The injected water gradually sweeps the LP layer (Figure 4.13a), so that after 1.5 PV of water flooding, almost one third of the LP layer is affected by the injected water. The water profile in the LP layer will affect the performance of the later treatments as described below.

Figure 4.14 compares water saturation profiles at 3 PV of water injection under the effects of near wellbore and in-depth gel treatments, performed at 1.5 PV. As shown in Figure 4.14, the water saturation profiles are considerably different after the two treatments. One of the main evident differences between the two cases is where the water cross flow happens, which are illustrated in Figures 4.14a and b using arrows. In the case of near

wellbore treatment, the water which was injected after near wellbore treatment, first flows to the LP layer due to high resistance in the HP layer created by the gel around the wellbore. However, it cross flows back through the LP water swept zone (Figure 4.13a) to the water channel right after the gel position (Figure 4.14a). By comparing Figures 4.14a and b, it is observed that the dark blue area in the LP layer around the wellbore, which has the maximum water saturation ($0.75 < s_w < 0.8$), is thicker for the near wellbore case than that of the in-depth treatment. This area is where the major water cross flow happens in the case of near wellbore treatment, marked also by an arrow in Figure 4.14a.

However for the case of in-depth treatment, the position of the major water cross flow is identified at the middle of the LP layer just around the treated zone. The injected water first flows into the HP layer, then is diverted to the LP layer as it approaches high resistance gel positions. It is again cross flows back to the water channel right after the treatment region. As shown in Figure 4.14b, the deeper water diversion and cross flow in the case of in-depth treatment has resulted in a more effective water sweep, compared to the near wellbore treatment (Figure 4.14a).

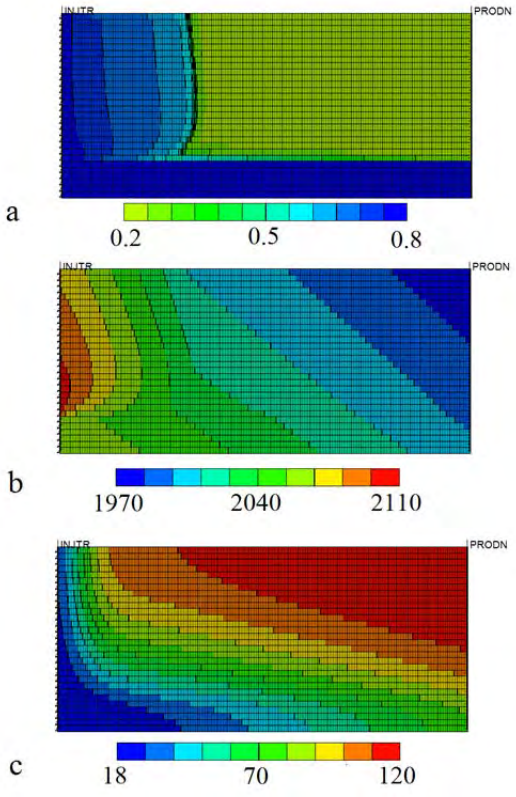

Figure 4.13. Snapshots of a) water saturation, b) pressure (psi) and c) temperature (^{o}C) for the two layered reservoir with free cross flow after 1.5 PV water injection. In this reservoir, permeability ratio=100, h/H=0.2, k_v/k_h=0.01, viscosity ratio=1.

Therefore, it is more effective to treat the HP layer in a position deeper than the water front in the LP layer (Figure 4.13a). Near wellbore treatment or even treatments in a shallow depth may result in an immediate water cross flow back to the water channel through the portion of the LP layer which has previously been swept by water; while treating in depth of the reservoir will delay the water cross flow. Figure 4.15 compares the performances of the methods in enhancing oil RF and reducing water cut%. Although both near wellbore and in-depth methods enhance oil RF of water flooding, the in-depth

treatment is more efficient. The in-depth gel treatment results in a steeper decrease in water cut and a steeper increase in oil RF. An incremental oil RF of about 7% is obtained by the in-depth treatment after 5 PV water flooding, almost 1.5% higher than the near wellbore treatment.

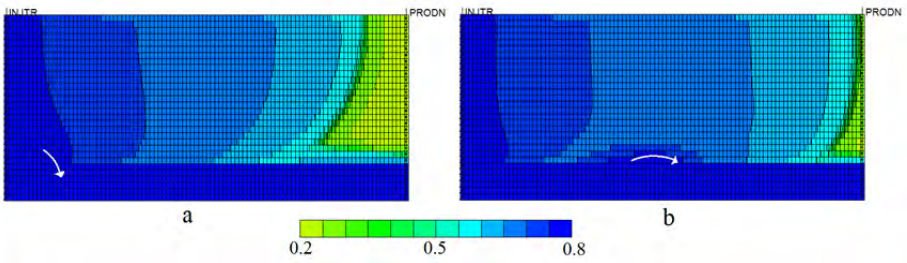

Figure 4.14. Snapshots of water saturation in the two-layered reservoir with free cross flow at 3 PV water flooding for two cases: a) near wellbore gel treatment at 1.5 PV and b) in-depth gel treatment at 1.5 PV. Arrows show the position of major cross flow.

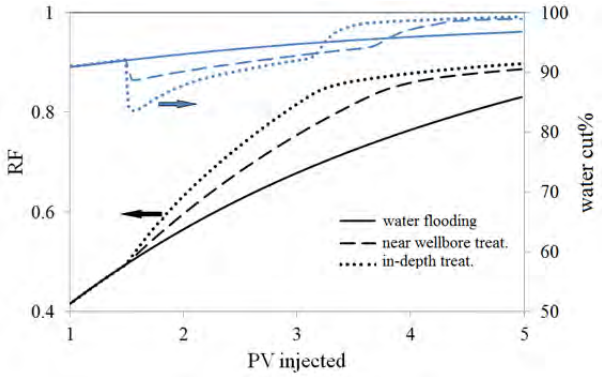

Figure 4.15. Oil recovery factor and water cut% as functions of the injected PV in the two-layered reservoir with free cross flow for different cases: continued water flooding, near wellbore gel treatment at 1.5 PV and in-depth gel treatment at 1.5 PV.

Figure 4.16 confirms the major effect of water cross flow on the performance of near wellbore and in-depth treatments. The obtained RF for both treatment approaches are compared in two different reservoirs, a reservoir without cross flow (Figure 4.16a) and another one with cross flow in which k_v/k_h=0.1

(Figure 4.16b). It can be seen that when cross flow is absent (e.g., due to a continuous impermeable barrier separating the layers), the oil RF resulted from near wellbore and in-depth treatments are almost equal. However, in the case of reservoir with free cross flow and high vertical permeability (k_v/k_h=0.1), the near wellbore treatment is considerably less effective than the in-depth treatment. As discussed in section 4.1.2, vertical permeability increases the flow communications between the layers. High cross flow between the layers results in an evident difference in the performances of the near wellbore and the in-depth gel treatments. RF profile for the near wellbore treatment is close to that of water flooding of untreated reservoir, since the injected water cross flows back to the HP layer right after the treatment area around the injection well. While, in-depth treatment reduces the effect of cross flow in a larger distance. The incremental RF at 5 PV is more than 6% for in-depth treatment, compared to the near wellbore method.

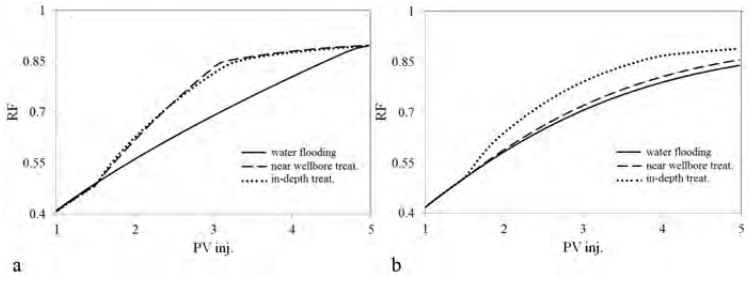

Figure 4.16. Oil recovery factor as a function of the injected PV in the two-layered reservoir for water flooding of untreated reservoir, near wellbore gel treatment at 1.5 PV and in-depth gel treatment at 1.5 PV. The results are shown for two different cases: a) reservoir without cross flow and b) reservoir with cross flow where k_v/k_h=0.1.

The pressure distribution in the reservoir after water flooding is affected by both the gravity (hydrodynamic pressure) and the water injection (medium flow resistance), as shown in Figure 4.13b. The maximum pressure happens

around the injector at the bottom of the LP near the HP layer. Near wellbore treatment is conducted in the high pressure-gradient zone of the reservoir, hence affects the injectivity of the reservoir; while, the in-depth treatments which are normally performed away from high pressure region, possess a minimal effect on the injectivity after treatment, as also pointed out by Fletcher et al. (1992).

High pressure gradients around the wellbore as well as high flow velocity in this region result in high shear rates close to the injection well. Figure 4.17 shows the shear rate as a function of the normalized radial distance from the wellbore in the LP and the HP layers. Shear rate in a porous medium is a direct function of the injection flow rate and an inverse function of the radial distance, medium thickness and square root of medium permeability (Lake, 1989; Sorbie, 1991). As shown in Figure 4.17, shear rate is considerably higher in the HP layer, compared to the LP layer mainly due to higher flow rate of the injected water in this layer. It can be seen that the shear rate in this layer is almost 1000 s^{-1} around the well and decreases to very low values (<0.1 s^{-1}) at the middle of the reservoir.

The injected solution for gel treatments experiences different shear rates during the injection process. High shear rate in the wellbore, especially through the well perforations, high shear rate in the porous media around the wellbore, and low shear rate at further distances from the injector. Depending on the position of the treatment, the shear rate history of the injected material would be different. For a near wellbore gel placement, the treatment is performed in a region with average high shear rates (>100 s^{-1}), while in the case of in-depth treatments, the average shear rate in the region is considerably less. Shear rate affects the gel kinetics, hence the treatment performance.

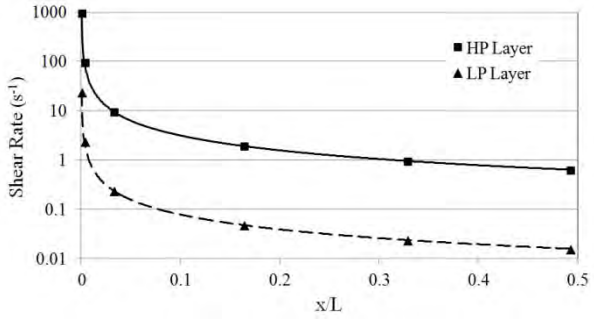

Figure 4.17. Shear rate as a function of the normalized radial distance for the LP and the HP layers.

Figure 4.18 compares the pressure distributions after the near wellbore and the in-depth gel treatments. The maximum pressure in the reservoir with in-depth treatment is higher than that in the case with near wellbore treatment. This higher pressure is related to the higher water sweep efficiency in the LP layer for the case of the in-depth treatment (Figure 4.14). Moreover, the pressure profiles are completely different for the two treatments, due to different flow profiles. As discussed above, water cross flow from the LP to the HP layer happens close to the injection well in the case of near wellbore treatment, which can be also identified by the form of the pressure contour lines (shown with an arrow in Figure 4.18a). In the case of in-depth treatment, however, pressure contour lines show water cross flow from the HP layer to the LP layer behind the gel and the cross flow back after the gel position (shown with an arrow in Figure 4.18b).

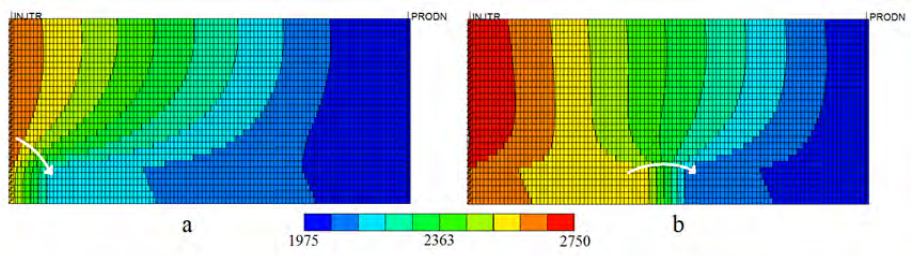

Figure 4.18. Snapshots of pressure (psi) distribution in the two-layered reservoir with free cross flow at 3 PV water flooding for two cases: a) near wellbore gel treatment at 1.5 PV and b) in-depth gel treatment at 1.5 PV. Arrows show the position of major cross flow.

Temperature profile in the reservoir is another parameter which affects the reservoir treatments. As shown in Figure 4.13c, water flooding for 1.5 PV has created a temperature gradient in the reservoir, especially in the HP layer. It can be seen that the near wellbore area has low temperature, < 30 ^{o}C, while the middle of the HP layer, the in-depth treatment distance, has a temperature of about 50 ^{o}C. High temperature affects the gelation kinetics. This demonstrates the importance of taking temperature effect factor into account in the case of the in the in-depth treatment.

As a conclusion in this section, although in-depth profile modification is a challenging process, but often is more effective than the near wellbore treatments in enhancing oil recovery in the layered reservoirs which have permeability contrast and free cross flow between their layers. As discussed in more detail in section 1.2, Na-silicate is potentially an attractive candidate for reservoir in-depth profile modifications, provided that its behavior is fully understood under different reservoir conditions. Next section is devoted to report the quantitative laboratory study done on Na-silicate to evaluate the main factors that affect Na-silicate gel properties during the reservoir in-depth placement.

4.2. Evaluation of alkaline sodium silicate properties

Alkaline sodium silicate properties, including interfacial tension with oil, viscosity, gel time, strength and shrinkage are addressed in this section.

4.2.1. Effect of sodium silicate on interfacial tension

Similar to other alkaline solutions, Na-silicate decreases water oil interfacial tension (σ). The effect of Na-silicate content on the interfacial tensions with different types of synthetic oils such as *n*-C_{10}, *n*-C_{10}+0.01 M NN-DMDA and *n*-C_{10}+ NN-DMDA + toluene + asphaltene were addressed. The interfacial tension data were normalized by $\sigma_n = 1 + (\sigma - \sigma_0)/\sigma_{0,n-C_{10}}$ for different oil types, where σ_0 is the interfacial tension between each of synthesized oil and DW (zero Na-silicate content), and $\sigma_{0,n-C_{10}}$ is the interfacial tension between *n*-C_{10} and DW (≈ 46 dyne/cm).The obtained σ_n data are plotted against Na-silicate content and presented in Figure 4.19. In general, σ_n was reduced with Na-silicate content. Above about 3 wt%, the effect of Na-silicate content on the interfacial tension decreased. This is also the case for pH variations versus Na-silicate content, where pH demonstrates a marginal change at Na-silicate contents above 3 wt%.

At a given pH, Na-silicate solutions showed considerably lower interfacial tension, compared to NaOH. For example 0.012 wt% NaOH solution has the same pH as 5 wt% Na-silicate solution (pH≈11.3); however, the interfacial tension between synthesized oil of *n*-C_{10}+ NN-DMDA + toluene + asphaltene is about 1 and 13.7 with Na-silicate and NaOH, respectively.

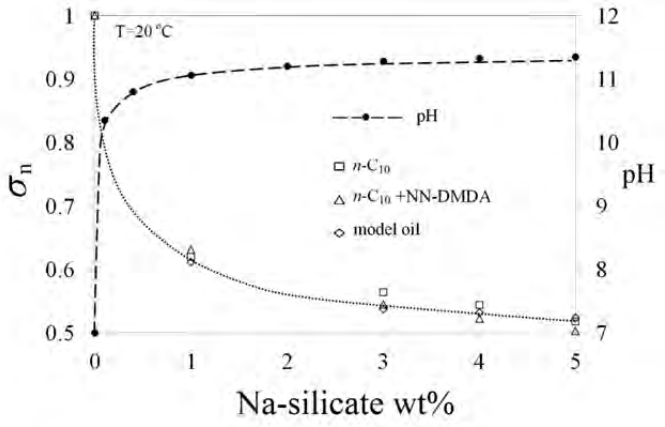

Figure 4.19. pH and normalized interfacial tension as a function of Na-silicate content.

4.2.2. Factors affecting gel setting time

Factors that affect Na-silicate gel setting time are the silicate content, the pH, the concentration of divalent ions (namely Ca^{2+} and Mg^{2+}), temperature and the shear rate (Krumrine and Boyce, 1985). This section addresses the influence of each factor on gelation time, and then the combined effect, in an attempt to predict Na-silicate gel setting time.

Typical viscosity profiles for 4.5 wt% Na-silicate with pHs of 10.30 and 10.40 at 10 sec^{-1} and room temperature (20 °C) are presented in Figure 4.20. Na-silicate solution with reduced pH has water-like viscosity (between 1.2 to 2 cp, depending on the silicate content) just after pH adjustment. Viscosity increases gradually in a linear trend as a function of time until gel time, in which viscosity starts to highly increase. The maximum viscosity before gelation is around 5 cp, indicating good injectivity prior to gelation. Gelation time (t_g) is defined here as the time after which viscosity deviates from linearity. Based on this definition, gel times of the studied samples in Figure 4.20 are approximately 140 and 480 for pH of 10.30 and 10.40, respectively.

As it can be seen in Figure 4.20, the onset of gelation is followed by fluctuations in viscosity. Lakatos et al. (2009) referred to this as an induction period. For both pH values, a slight reduction in viscosity is followed by a continued increase in viscosity. This may suggest the occurrence of a localized increase in pH caused by the OH^-, produced from the condensation reaction presented by Eq. (1.2).

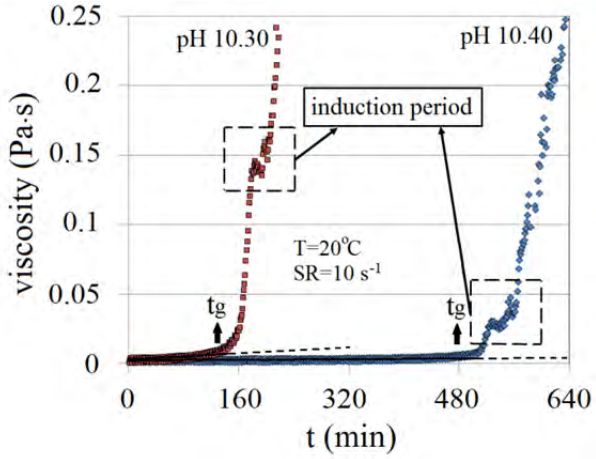

Figure 4.20. Viscosity profiles for 4.5 wt% Na-silicate solution at pH values of 10.30 and 10.40 as a function of time after the pH adjustment.

Figure 4.21 demonstrates the combined effects of Na-silicate content and pH on gel setting time at 20°C and a shear rate of 10 sec^{-1}. Using Figure 4.21, the amount of acid that has to be added to silicate solutions to reach a certain gelation time can also be estimated. In this plot, gelling times are presented as iso-gelation time contour lines for Na-silicate contents of 3-6 wt%.

The profile of pH versus HCl concentration for all the Na-silicate contents shows a typical trend, where pH decreases linearly up to a certain point (called here the deviation point), after which the rate of pH reduction increases with the added acid. However, the gradient of pH reduction as a

function of HCl concentration depend on the Na-silicate content, i.e., the higher the Na-silicate wt%, the lower the gradient, indicating the increase in buffer capacity. It is also demonstrated that the deviation point is also dependent to the Na-silicate content. As an example, for 3 wt% Na-silicate solution, the deviation occurs at about pH 10.7, corresponding to the addition of 0.1 M HCl, whereas the deviation point for 6 wt% Na-silicate solution occurs at pH 10.4, which corresponds to an acid concentration of 0.25 M.

As shown in Figure 4.21, for a specific pH, the gelation time decreases with silicate content, due to the increase of the condensation rate of silicic acid. As an example, reducing pH of 6 wt% from 11.35 to about 10.55 brings gelation time to roughly 100 min, while it exceeds 10000 min at a pH of 10.55 for 3 wt%. Lowering the pH for a given silicate content also reduces gel time due to the increased silicic acid condensation, see Eq. (1.2).

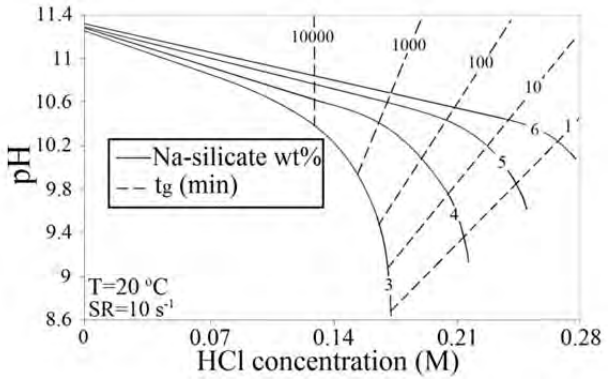

Figure 4.21. The HCl concentration that has to be added to different silicate contents (3, 4, 5 and 6 wt % in DW) at 20°C and a shear rate of 10 sec^{-1} to adjust the pH for achieving the desired gel time.

For the 4.5 wt% Na-silicate solution, precipitation appears at Ca^{2+}/Mg^{2+} concentrations > 1500 ppm. Addition of SSW (Table 3.1) to Na-silicate solution results in immediate white precipitation, which is believed to be

caused by the formation of calcium and magnesium silicate (Krumrine and Boyce, 1985). The precipitation produced by adding 25 wt% of SSW to 4.5 wt% Na-silicate solution causes the solution viscosity to increase to about 100 cp at 20°C and a shear rate of 10 s^{-1} prior to gel onset. A slight reduction in pH to 10.90 (by adding less than 0.1 M HCl) results in an immediate gelation in addition to precipitation.

No precipitation was observed for LSW (obtained by 25 times dilution of SSW), indicating LSW potential for being used as pre and post-flush in the field application of Na-silicate. A comparison is made for the gelation times of 4.5 wt% Na-silicate solution which is prepared with LSW and modified LSW (without Ca^{2+} and Mg^{2+}) in Figure 4.22. The gelation time is presented as a ratio of t_{g0}, which refers to the gelation time at zero salinity and room temperature. Figure 4.22 shows that the average ratio between gelation times of solution made by LSW and DW at different pH values is approximately 0.4; while this average ratio for the solution made by divalent ion-free LSW is greater than 0.7, as shown in Figure 4.24. Considering the lower relative concentrations of Ca^{2+} and Mg^{2+} in LSW compared to Na^{+} and K^{+} (almost 0.2), Figure 4.22 confirms the greater influence of the divalent ions in charge screening and reduction of dielectric constant of the solution.

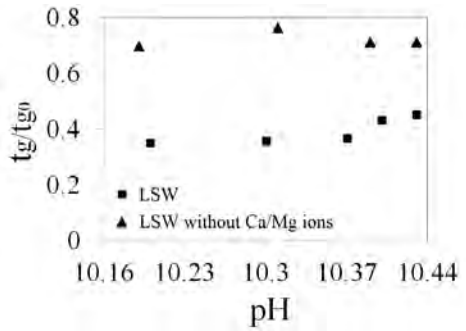

Figure 4.22. t_g/t_{g0} for 4.5 wt% Na-silicate dissolved in LSW with and without Ca^{2+} and Mg^{2+} as a function of the solution pH.

To evaluate the individual and combined effects of Ca^{2+} and Mg^{2+} on Na-silicate gelation, viscosity versus time of 5 wt% Na-silicate solution at pH 10.70 is compared in Figure 4.23 for three different cases: 0.0165 M Ca^{2+}, 0.0165 M Mg^{2+} and 0.00825 M Ca^{2+}+0.00825 M Mg^{2+}. The ion-free solution gels after about 50 h. The solution which contains just Ca^{2+} has the shortest gelation time ($t_g \approx 1$ h), while the one with Mg^{2+} gels after about 1.5 h. Gelation time for the combined ions lies between the times for the two individual ions. The larger effect of Ca^{2+} compared with Mg^{2+} may be caused by the greater effect of calcium ions on the dielectric constant. For practical purposes in predicting gelation time, however, the effect of both ions is considered to be equal.

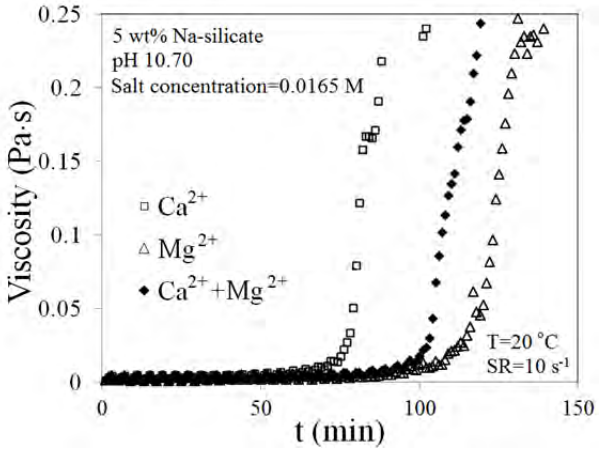

Figure 4.23. Viscosity as a function of time for a 5 wt% Na-silicate solution with a pH_i of 10.70 containing 0.0165 M of Ca^{2+}, Mg^{2+} and equivalent both ions.

As defined earlier, the gelation time of a given Na-silicate solution at zero salinity (ion-free) and room temperature (20°C) is considered as a reference gel time (t_{g0}). t_{g0} can be estimated using Figure 4.21 for Na-silicate contents in the range of 3 to 6 wt% and with different pH values. The impacts of

temperature and divalent ions' concentration on normalized gel time (t_g/t_{g0}) are depicted in Figure 4.24 in a semi-logarithmic plot. The experiments were done for Na-silicate solutions containing 4.5 and 5 wt% Na-silicate with different pH values of 10.30 and 10.40.

As shown in Figure 4.24, by increasing divalent ions' concentration at a temperature of 20°C, the normalized gel time of Na-silicate solution decreases almost with a linear trend for different tested samples. Addition of 0.018 M divalent ions will result in almost 100 times reduction of gel time.

The semi-logarithmic plot of t_g/t_{g0} as a function of the reciprocal absolute temperature (Arrhenius type plot) shows that the temperature effect on gelation time below 40°C (313 K) is smaller than that for the higher temperatures, in the tested pH range (Figure 4.24). A similar observation has previously been reported (Kristensen et al., 1993; Iler, 1979; Stavland et al., 2011a). According to Iler (1979), the drop in activation energy in this range implies that there is a pre-equilibrium step in the polymerization. First, some small polymeric species are formed with which the monomer reacts preferentially. This is a kind of induction period. Activation energy for temperatures above 40°C is estimated to be approximately 70 kJ/mole. This is in good agreement with the average activation energy (ranges between 60-80 kJ/mole) reported in the literature (Jurinak and Summers, 1991; Iler, 1979; Stavland et al., 2011a).

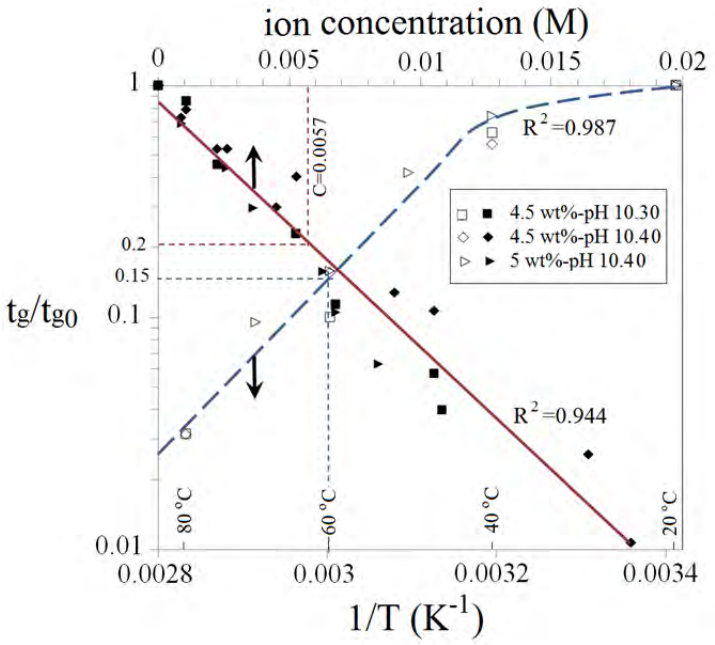

Figure 4.24. Normalized gelation time (t_g/t_{g0}) as a function of the reciprocal absolute temperature and divalent ions' concentration for 4.5 and 5 wt% Na-silicate solutions with different pH values.

Figure 4.21 and Figure 4.24 together can be used for approximating the combined effects of Na-silicate content, pH, temperature and divalent ions' concentration on the gel time. t_{g0} is first approximated using Figure 4.21 under the effects of Na-silicate content and pH. The individual effects of temperature and divalent cations on the normalized gel time (t_g/t_{g0}) are then found using Figure 4.24. These individual effects are finally combined by simple multiplication. Table 4.1 clearly summarizes this method in estimating gelation times for four different Na-silicate samples. The method is described here with an example (the first sample in Table 4.1). Gelation time is predicted for 4 wt% Na-silicate at a pH of 10.40, which contains 400 ppm $CaCl_2$ and 200 ppm $MgCl_2$ and is heated to 60 °C. The gelation time of 4 wt% Na-silicate with a pH of 10.40 at T=20 °C and zero salinity is first estimated using Figure

4.21 to be t_{g0}=1000 min. The normalized gelation time is then obtained for the effect of temperature, $\left(t_g / t_{g0}\right)_T$. As indicated in Figure 4.24 with a blue dashed line, $\left(t_g / t_{g0}\right)_T = 0.15$ when T=60 °C. The effects of $CaCl_2$ and $MgCl_2$ are included by first converting their concentrations in the solution to the molar concentration (M) and then summing the concentrations, giving C_{total}=0.0057 M. As indicated in Figure 4.24 with a red dashed line, $\left(t_g / t_{g0}\right)_{ion} = 0.21$ when C_{total}=0.0057. The gelation time of this sample can be estimated now by a simple equation as

$$t_g = t_{g0} \times \left(\frac{t_g}{t_{g0}}\right)_T \times \left(\frac{t_g}{t_{g0}}\right)_{ion} = 31 \qquad (4.1)$$

The experimental gelation time for this sample was obtained by viscosity measurement as t_g=33 min. Reasonable precision is obtained with this method, which could be regarded as a first-hand prediction of gelation time for practical applications.

Table 4.1. Summarized method for estimating gelation time applied to four different Na-silicate samples. Estimated gelation times are compared with the experimental results.

Na-silicate (wt%)	pH	T (°C)	$CaCl_2$ (ppm)	$MgCl_2$ (ppm)	t_{g0} (min), Figure 4.21	t_g/t_{g0} due to T, Figure 4.24	t_g/t_{g0} due to ion, Figure 4.24	Estimated t_g (min) Eq. (4.1)	Experimental t_g (min)
4	10.40	60	400	200	1000	0.15	0.21	31	33
5	10.55	50	250	250	520	0.32	0.25	42	45
5	10.70	45	200	350	2400	0.47	0.22	248	215
6	10.80	70	800	0	3800	0.065	0.13	32	26

In practice, Na-silicate solutions are exposed to different shear rates both during injection and during flow through the porous media in the reservoir. Different correlations have been suggested for relating the shear rate to flow rate, reservoir thickness, porosity and permeability (Sorbie, 1991). Based on the estimated typical shear rates for the reservoir, an average value of 10 s^{-1} was used for viscosity measurements and gel time determination in this work, as indicated in the previous sections. This section addresses the effects on the viscosity and gelling time, when Na-silicate is exposed to a high shear rate before gelling time, which is the case in the wellbore during injection in the porous media, and after gelling time, which may happen by imposing high pressure behind the gel in the reservoir.

Figure 4.25a shows a comparison of the viscosity profiles for 4.5 wt% Na-silicate with pH 10.30 for different constant shear rates (10 and 1000 s^{-1}) and a combined shear rate (1000 s^{-1} for 1 h, then 10 s^{-1}). Viscosity profiles and gel setting times are completely different for constant shear rates of 10 and 1000 s^{-1}. The studied Na-silicate sample gels at about 140 and 110 min, as exposed to shear rates of 10 and 1000 s^{-1}, respectively. So the gel setting time is accelerated (almost half an hour) for this sample as the shear rate increases from 10 to 1000 s^{-1}. At a shear rate of 1000 s^{-1} after gelation time, the viscosity of the gel does not exceed 25 cp. This may be explained by the effect of high shear rates in disturbing the gel network. The initial gradient of viscosity just after the gelation time is observed to be lower at higher shear rates.

When viscosity profiles in Figure 4.25a are compared for constant shear rate of 10 s^{-1} and combined shear rate of 1000 s^{-1} for 1 h then 10 s^{-1}, it is observed that imposing high shear rate (1000 s^{-1}) for a limited period of time (in this test 1 h) after pH adjustment and before gelation, accelerates the gel time of

the tested sample for almost 15 min. This observation shows that estimation of the gelation time must be corrected for the effect of the shear rate history to which the Na-silicate solution has been exposed to after pH adjustment.

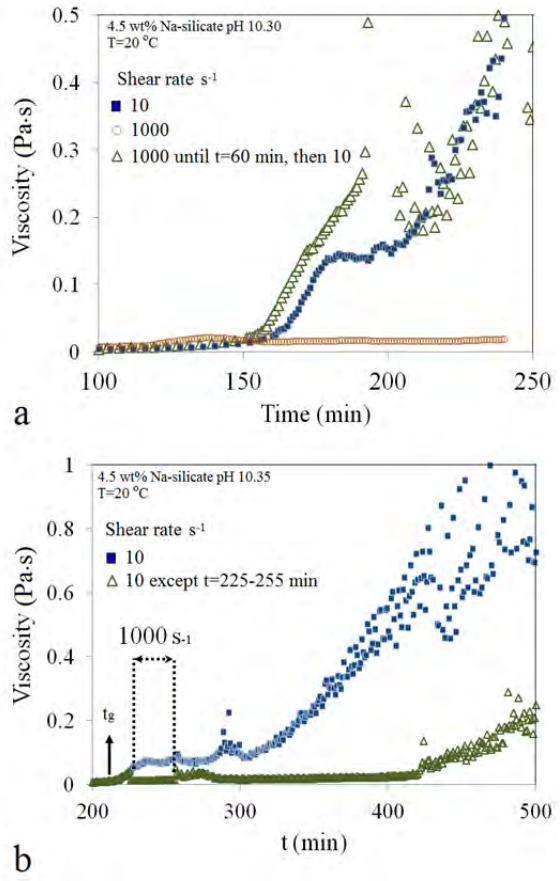

Figure 4.25. Viscosity profiles for a) 4.5 wt% Na-silicate with a pH of 10.30 for shear rates of 10 and 1000 s^{-1} and combined shear rate of 1000 s^{-1} for 1 h, then 10 s^{-1} and b) 4.5 wt% Na silicate with a pH of 10.35 which is exposed to 30 min high shear rate (1000 s^{-1}) after gel time at t=225 min in comparison with constant low shear rate (10 s^{-1}).

The effect of imposing high shear rate after gelation time on the viscosity profile of Na-silicate is also investigated. Two different cases are compared for 4.5 wt% Na-silicate with a pH of 10.35 (Figure 4.25b). In the first case, a

constant low shear rate of 10 s^{-1} was applied. In the second case, the initial shear rate was 10 s^{-1}, as in the first case, but at t=225 min (15 min after gelation time), a high shear rate (1000 s^{-1}) was imposed suddenly for a time period of 30 min and then shear rate decreased again to 10 s^{-1}. It can be seen that the viscosity of the gel did not increase as the first case after imposing high shear rate. Viscosity stabilized at a low value after removing the high shear rate in the second case. After some time (about 3 h), however, viscosity started to increase with the same gradient as observed in first case after gel time.

This observation demonstrates that a high shear rate after gelation can break the formed polymeric bonds, hence stabilize the viscosity at a certain value. The observed increase in the viscosity at a later time after removing high shear rate may imply a secondary gelation process. This observation can be useful in the case of failure in placing the injected gel in the field applications. It is possible to disturb the newly formed loose gel by imposing high shear rate. This will result in a secondary gelation at a later time, hence new position.

4.2.3. Gel strength

Typically, the gel strength of Na-silicate increases after gel time and then stabilizes at a maximum value, which is called here maximum gel strength. The time in which the gel strength stabilizes at its maximum is called t_{mgs}.

The effects of pH and Na-silicate content on gel strength are shown in Figure 4.26. The iso-gelation time contour lines are also illustrated in Figure 4.26. Corresponding values of t_{mgs} for different gelation times are also shown in Figure 4.26, which means that t_{mgs} for different Na-silicate samples is a function of t_g. Figure 4.26 shows that for a given Na-silicate content, the gel becomes stronger and t_{mgs} becomes shorter as the pH decreases. At a pH of

10.10 for 3 wt% Na-silicate solution, for example, a loose gel is obtained (maximum strength <100 Pa) after more than 6 days, whereas 6 wt% produces a gel 30 times stronger (>3000 Pa) after just 1 h.

As shown in Figure 4.26, at a given Na-silicate content, a longer gelation time leads to a weaker gel. At a certain gelation time, higher silicate content produces a stronger gel. Although both 6 wt% Na-silicate at a pH of 10.20 and 3 wt% Na-silicate at a pH of 8.70 gel after 1 min, for instance, the maximum gel strength of 6 wt% is 2800 Pa, which is almost 4 times of the strength of 3 wt% (700 Pa). However, as pointed out above, t_{mgs} for both samples are almost equal, due to equal gelation times.

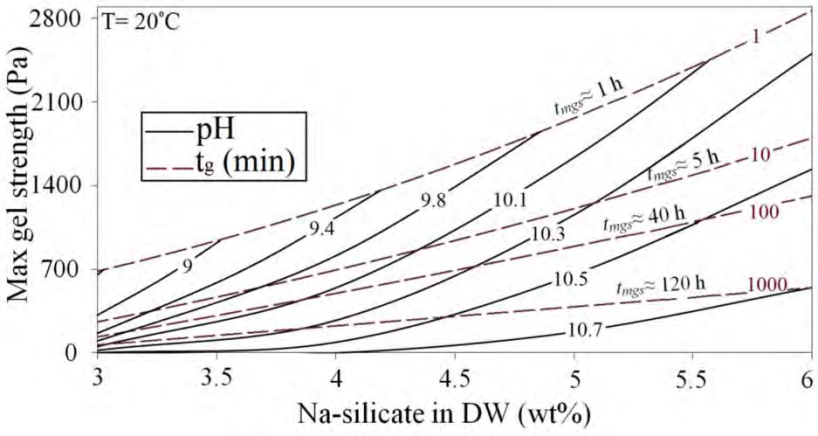

Figure 4.26. Maximum gel strength as a function of Na-silicate (wt%) and pH. The iso-gelation time contour lines and corresponding t_{mgs} values are illustrated.

The effect of temperature on the gel strength for 4.5 wt% Na-silicate with a pH of 10.30 is illustrated in Figure 4.27 for temperatures of 20, 50 and 80°C. Gel samples which are kept at elevated temperatures have lower maximum gel strength than the one at 20°C. Trapped bubbles were observed in the elevated temperature experiment, which may have disturbed the continuity of the gel's

network, and hence reduced gel strength. However, this does not adequately explain the increase of gel strength at 80°C compared with 50°C. This phenomenon is perhaps better explained by the fact that increasing the temperature to 80°C increases silicate solubility. This in turn causes a reduction in the pH, hence accelerating gel formation and consequently increasing gel strength compared to the sample at 50°C. This is consistent with the syneresis experimental results for the temperature effect, which are presented in the next section.

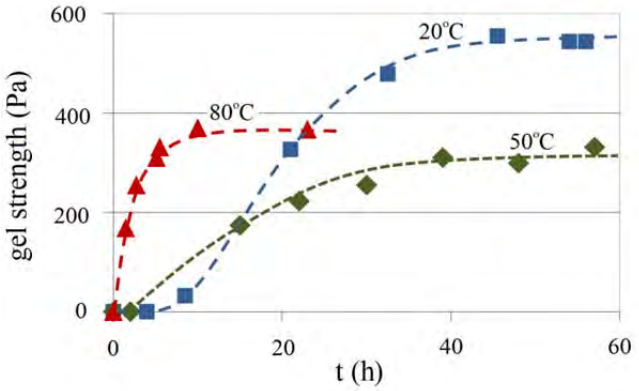

Figure 4.27. Gel strength as a function of time for 4.5 wt% Na-silicate with a pH of 10.30 at different temperatures of 20, 50 and 80°C.

The effect of divalent ions on the maximum gel strength is shown in Figure 4.28 for 4.5 wt% Na-silicate solution with a pH_i of 10.30 (pH of ion-free solution). As Ca^{2+} or Mg^{2+} concentration increases, gel strength increases and t_{mgs} decreases. In the absence of Ca^{2+} and Mg^{2+}, Na-silicate gel reaches its maximum strength of 500 Pa after about 40 h, whereas maximum gel strength reached 1500 Pa and t_{mgs} decreased to 5 h when the Na-silicate solution was prepared in the presence of 0.01 M $MgCl_2$. Figure 4.28 indicates that both ions similarly enhance the gel strength with almost a linear trend. At the same concentrations, however, Mg^{2+} can be seen to be relatively less effective than

Ca^{2+} in enhancing gel strength. That agrees with the observation made for gelation time in Figure 4.23.

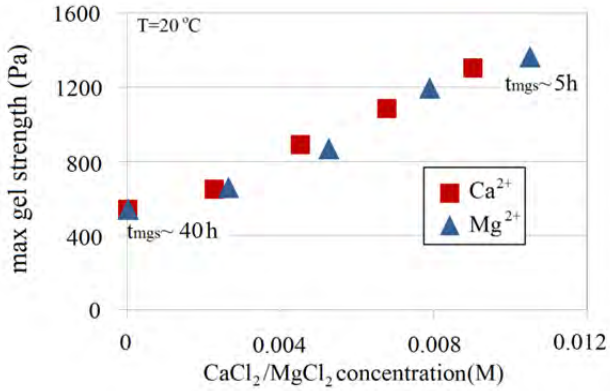

Figure 4.28. Maximum gel strength as a function of Ca^{2+} and Mg^{2+} molar concentrations for 4.5 wt% Na-silicate with pH_i of 10.30.

4.2.4. Gel shrinkage

There are normally three successive stages in a Na-silicate gel life: after pH adjustment until abrupt viscosity increase (t_g), from gel setting time to gel network formation equilibrium (t_{mgs}) and finally gel shrinkage and liquid expulsion. There is a period after gelation time, in which no shrinkage occurs. This observation has also been reported by Brinker and Scherer (1990). It was realized in this work that this time period is between t_g and t_{mgs}, when the formed gel approaches equilibrium at its maximum strength.

The expelled liquid (wt %) as a function of time for 4, 5 and 6 wt% Na-silicate at pHs of 10.10 and 10.50 are compared in Figure 4.29. For a given pH, increasing silicate content (%wt) accelerates gel shrinkage. For example, Figure 4.29 shows that 6 and 4 wt% Na-silicate samples with pH 10.10 start to shrink at approximately 1 and 80 h, respectively. At a given pH, the higher the silicate content, the higher the rate of shrinkage and total shrinkage. This is in agreement with the reported observations (Holmes et al., 1919; Ferguson and

Applebey, 1930; Brinker and Scherer, 1990). For a 6 wt% Na-silicate solution at a pH of 10.10, for instance, the initial rate of shrinkage and the total shrinkage at t=400 h are 0.1 wt% per hour and 25 wt% respectively. For 4 wt% Na-silicate at the same pH, the initial rate of gel shrinkage and the total shrinkage at *t*=400 h are approximately 0.025 wt% per hour and 8 wt% respectively. At a certain Na-silicate content, lower pH results in earlier shrinkage and a higher shrinkage rate.

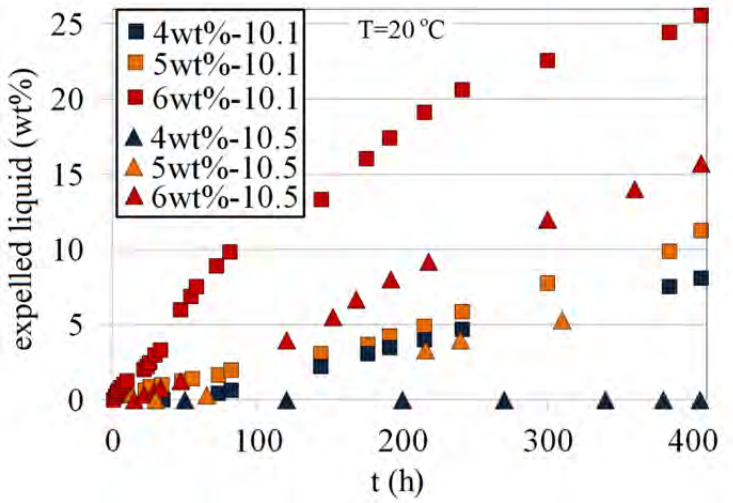

Figure 4.29. Weight percent of the expelled liquid as a function of time for 4, 5 and 6 wt% Na-silicate solutions with pHs of 10.10 and 10.50 respectively at 20°C.

To address the effect of temperature on syneresis, the gel of 4.5 wt% at a pH of 10.30 was kept at three different temperatures of 20, 50 and 80 °C. The expelled liquid wt % is shown in Figure 4.30. It was observed that syneresis of a given sample at elevated temperatures started sooner than its corresponding t_{mgs}. As an example, t_{mgs} for 4.5 wt% Na-silicate with pH of 10.30 at 80°C is about 10 h (see Figure 4.27), while its shrinkage starts earlier than 5 h (about half its t_{mgs}), as shown in Figure 4.30. Temperature also increases the rate of shrinkage and ultimate shrinkage volume. Shrinkage rates

at 20, 50 and 80°C are approximately 0.013, 0.054 and 0.21 wt% per hour, respectively.

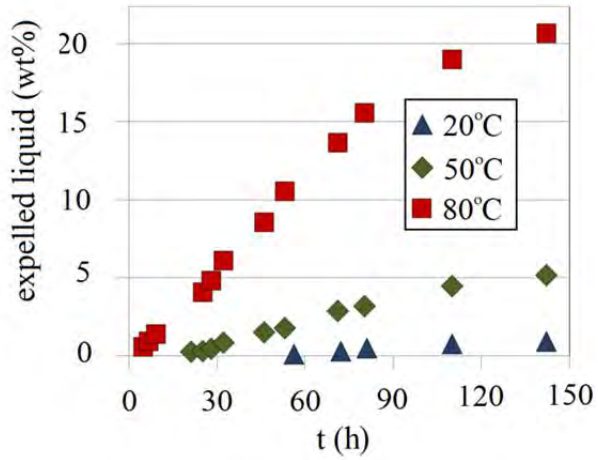

Figure 4.30. Weight percent of the expelled liquid as a function of time for a 4.5 wt% Na-silicate solution with a pH of 10.30 at temperatures of 20, 50 and 80°C.

Figure 4.31 shows the expelled liquid wt% for 4.5 wt% at a pH of 10.30 by addition of divalent ions (Ca^{2+} and Mg^{2+}). When Figure 4.31 is compared with Figure 4.30 at T=20 °C, it is observed that adding 0.009 M $CaCl_2$, increases the shrinkage by almost 10 times. The comparison of 0.009 M solutions with Ca^{2+} and Mg^{2+} reveals that presence of Mg^{2+} results in less gel shrinkage when added to the Na-silicate solution, compared with Ca^{2+}. This is in agreement with the observation made for gelation time and gel strength.

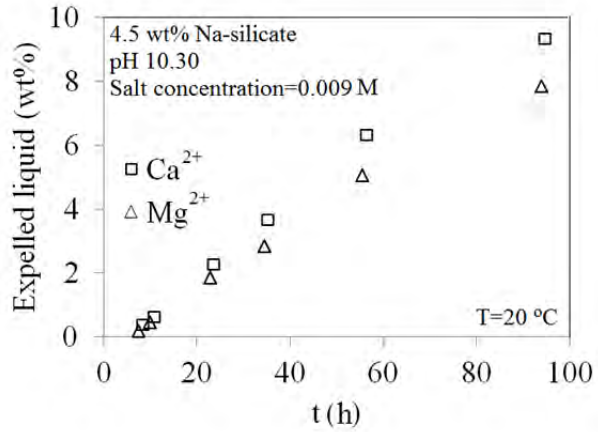

Figure 4.31. Weight percent of the expelled liquid as a function of time for 4.5 wt% Na-silicate solution with pH 10.30 at 20 °C. A comparison is made for 0.009 M solutions of $CaCl_2$ and $MgCl_2$.

It was observed that when the gel samples were prepared in polypropylene containers, syneresis mostly happened in the gel contact with the polypropylene container wall. The gel separated from the wall and was contracted to a compact mass at the center of the container. This may be explained by weak adhesion to the wall, which results in a lower energy level in the gel periphery (Bryant et al., 1996). When glass vials were used, however, the gel remained in contact with the vial wall and shrinkage was limited to the gel-air interface at the top of the vial. In this case, a considerably lower shrinkage was observed. This may be explained by possible chemisorption of silicate solution on the glass silicate. Lower shrinkage rates have been reported in silicate porous media (Bryant et al., 1996), which is qualitatively in agreement with our observation and may support the explanation given above.

Na-silicate gel properties were quantitatively investigated, using bulk measurements, for in-depth reservoir profile modifications. However, another important step before performing an in-depth treatment is to verify Na-silicate

gel performance when it is flowing through a porous medium. Dynamic conditions during transport in porous media may be completely different from static bulk measurements. Next section addresses Na-silicate behavior in porous media.

4.3. Sodium silicate behavior in porous media

It is important to evaluate Na-silicate injectivity, preferential flow path (possibility of leakoff into the matrix), adsorption/retention, gelation time, gel profile and strength in deep placements in porous media. Unconsolidated core flooding experiments were used to evaluate these parameters. Reservoir simulation was also done for better understanding of the mechanisms.

4.3.1. Flooding experiments in unconsolidated sand cores

Different lab-scale studies were conducted experimentally and numerically to address Na-silicate flow through porous media. Experimental studies were performed on long transparent tubes with sand-packs, described in section 3.2.2. The numerical simulation was done using STARS (CMG), described in section 3.3.2. For all the experimental studies in this section (except adsorption measurements which needed very low concentrations), 5 wt% Na-silicate solutions with different pH values were used. Bulk experiments showed that the Na-silicate samples with lower contents than 5 wt% would not produce strong enough gels for in-depth applications.

4.3.1.1. Evaluation of silicate dynamic adsorption

Adsorption of Na-silicate on surface minerals helps to determine the fraction of the injected Na-silicate that reaches the targeted treatment location in the reservoir.

Dynamic adsorption was evaluated by injecting a Na-silicate slug with the size of 0.48 PV in sand-pack A (Table 3.3), which was initially saturated with DW. The slug size was almost similar to what is later used for gel treatments in dual-permeability sand-packs. Two different Na-silicate solutions were studied which had silicon (Si) concentrations of 33 and 3.9 mg/l, which correspond to 0.0093 and 0.0011 wt% Na-silicate solutions, respectively. The low Si concentration in the tested solutions was used to precisely estimate the adsorbed amount. The concentration of silicon in the effluent was measured using ICP. The adsorption measurements are performed at room temperature.

The ratios between silicon concentrations in the effluent and the injected concentrations (C/C_0) are plotted against the injected pore volume (Figure 4.32a and b for the two concentrations of 33 and 3.9 mg/l, respectively). Commercial software CMG (STARS^{TM}, CMG User Manual, 2010), was used to match the experimental data. The matching parameter was adsorption density, as shown in Figure 4.32. The adsorption density was increased from 0 (for non-adsorbing material) to higher values, to match the experimentally obtained concentration curves. The simulation method addresses only the adsorption process and not the desorption process. In both cases, the experimental data were matched numerically only when it was assumed that Si adsorption takes place at (C/C_0) higher than 0.25.

The adsorption density was obtained from the numerical matched experimental data as shown in Figure 4.32. Figure 4.32a demonstrates that for C_0=33 mg/l, the best numerical match occurred when adsorption density is about 8.5e-10 kg/cm^3. In the case of C_0=3.9 mg/l (Figure 4.32b), the obtained adsorption density was about 4.5e-10 kg/cm^3. As silicon concentration in the injected slug increases from 3.9 to 33 mg/l (almost 8 times higher), the adsorption density is almost doubled.

Mono-layer adsorption density of silicon in sand pack A (with porosity of 0.45) was obtained as 1.4 e-8 kg/cm^3 by a simplified estimation. To estimate mono-layer adsorption, it was assumed that the average grain diameter in the sand-pack A is 200 μm. To simplify the calculations, the sand grains were considered to have spherical shape. It was also assumed that silicon is adsorbed in the form of silicate molecules (SiO_2) with atom radii of 0.16 *nm*, and the adsorption takes place on the total surface (including the contact area) of all the grains in the sand-pack. The experimentally obtained Si adsorption densities (Figure 4.32a and b) are more than ten times smaller than the estimated monolayer value. This demonstrates an inconsiderable Si adsorption on sand grain surfaces, especially at high Si concentrations, such as Na-silicate solutions which are used for gel treatments (5 wt% Na-silicate solution has Si concentration of 17000 mg/l).

Figures 4.32a and b show that Si adsorption is reversible. This is implied from the tails of the concentration profiles, which starts at (C/C_0) of about 0.25. It means that the adsorbed Si is desorbed in the post-flush water. The mass balance between the adsorbed and desorbed Si showed that most of the adsorbed mass is desorbed in the following water. For example, in the case of C_0=3.9 mg/l, the total adsorbed Si amount in the sand-pack is about 0.015 mg. If it is assumed that the desorption starts at 1.5 PV with an average concentration ratio of C/C_0=0.1 (as shown in Figure 4.32b), after about 2 PV, approximately 0.0065 mg (almost half) of the adsorbed mass is desorbed.

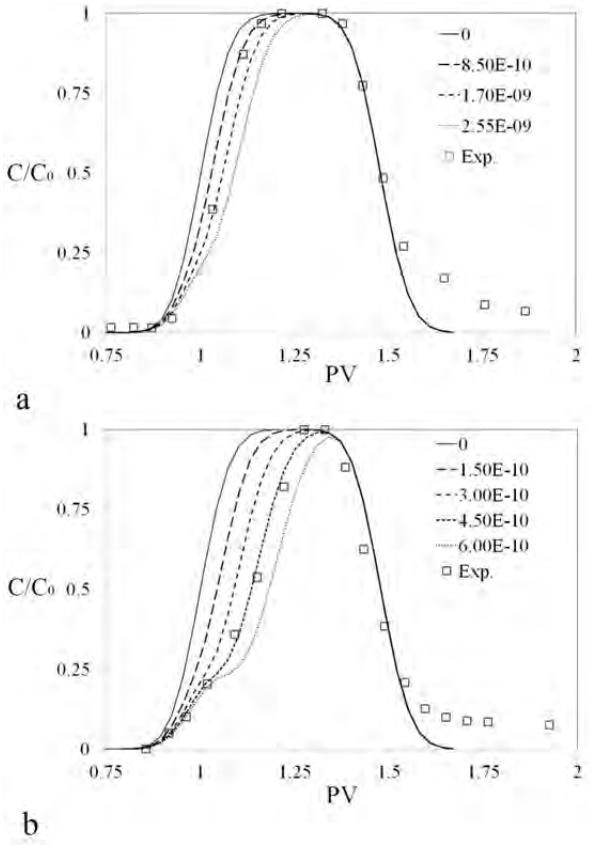

Figure 4.32. Comparison between the normalized effluent concentration data for 0.48 PV slug of Na-silicate solutions having silicon concentrations of a) 33 mg/l (0.0093 wt% Na silicate) and b) 3.9 mg/l (0.0011 wt% Na silicate) to determine the corresponding adsorption densities.

4.3.1.2. Sodium silicate dynamic gelation in porous media

Na-silicate is water soluble; hence it diffuses into the water during the transportation in the porous media. Furthermore, since there is density and viscosity contrasts between Na-silicate solution and fluid (water) in the porous media, the Na-silicate slug propagation is not piston like and the shape of the formed gel is not regular. A numerical sensitivity study was performed on the effects of physical diffusion, density and viscosity contrasts on the slug

propagation in porous media. Figure 4.33 compares the relative concentration (C/C_0) profiles of the injected solution slug at two different times and two different heights in the simulated medium, i.e., at the bottom (solid lines) and the top (dashed lines). The results are shown for two different solutions. First one (blue lines) only has density contrast with the water in the medium (density ratio= 1.2), while the other one (red lines) has both density and visosity contrast with the water in the medium (density ratio= 1.2, viscosity ratio=1.3). As shown in Figure 4.33, the injected slugs are diffused in water as they transport in the medium. The effect of numerical diffusion was minimized by small grid sizes. The effect of diffusion has to be considered in the design of in-depth treatments.

For a solution with density contrast of 1, the concentration profiles at the bottom and top of the medium coincide. However, when the solution density ratio increases to 1.2, gravity segregation affects the concentration profile as the slug propagates inside the porous medium (Figure 4.33 blue lines). The relative concentration profile is thicker at the bottom and thinner at the top. It causes the post-flush water to override the slug at later times. The effects of gravity segregation and water override are more pronounced as the height of the medium increases.

Figure 4.33 shows that the concentration profiles are also affected by viscosity contrast between the injected solution and the formation water (Red lines). It is observed that the viscosity contrast exacerbates the gravity segregation effect which increases the intensity of the water override. When the slug has a higher viscosity than the formation water, the flow resistance is higher wherever the slug is thicker. So since the slug is thinner at the top, due to the density contrast, flow resistance is lower there, compared to the bottom of the

medium. Hence the flow velocity is faster at the top and water override is accelerated.

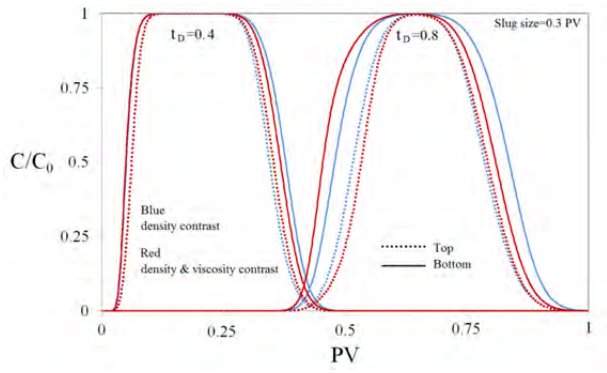

Figure 4.33. Concentration ratio at t_D=0.4 and t_D=0.8 for the injected slug in two different heights of the sand-pack, bottom (solid lines) and top (dashed lines). The results are shown for two different solutions: firs one (blue lines) has only density ratio=1.2 with the sand-pack initial water, while the second one (red lines) has both density ratio=1.2 and viscosity ratio=1.3 with the sand-pack initial water.

The Na-silicate gel profiles and strengths for different injected slug sizes are studied. 5 wt% Na-silicate at pH 10.40 were injected with different slug sizes, targeting the middle of the sand-pack A. Sand-pack is initially saturated with DW. The Na-silicate slug was injected at a rate of 0.1 ml/min, which is corresponding to the shear rate of about 10 s^{-1}. Silicate solution was placed almost at the middle of sand-pack with a DW post-flush. The injection rate was then reduced to 0.01 ml/min to monitor the gel formation by measuring the pressure drop between the inlet and the outlet. The results are compared for four different slug sizes of 0.35, 0.4, 0.45 and 0.5 PV. Figures 4.34a and b show the numerically and experimentally obtained profiles of the gel for different Na-silicate slug sizes after the gel placement at the middle of the medium. Figure 4.34a is a picture taken from the formed gel in the used transparent tubes after removing the sand in other parts using high pressure

air. There is a good agreement between the experimental (Figure 4.34a) and simulated (Figure 4.34b) results, which shows the ability of the developed numerical method in predicting the gel propagation and profile. The profile of the formed gel is dependent on the Na-silicate slug size. In the case of 0.35 PV slug size, most of the injected Na-silicate was diluted, mostly at the top due to gravity effect; so the formed gel has a small size. As the injected slug size increases, the formed gel sizes increased. For slug sizes $\leq$ 0.4 PV, water override was clear, while for the larger slug sizes, the gel fully occupies the sand-pack cross section.

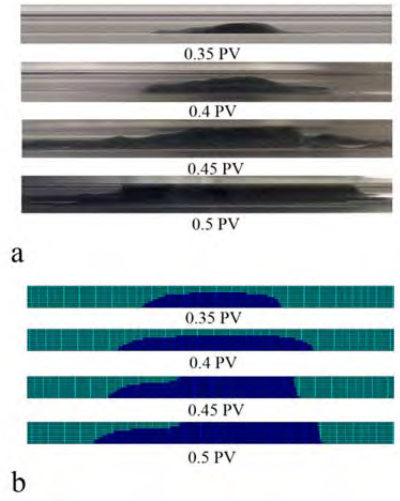

Figure 4.34. a) Numerically and b) experimentally obtained profiles of Na-silicate gel (5 wt% pH 10.42) injected in sand-pack A with different slug sizes of 0.35 PV, 0.4 PV, 0.45 PV and 0.5 PV.

Figure 4.35 compares the pressure build-up (flow resistance) during gel placements with different slug sizes. The bulk measured viscosity profile of 5 wt% Na-silicate at pH 10.40 is also presented in Figure 4.35. No considerable pressure increase is observed prior to Na-silicate gelation As shown in Figure 4.35, the pressure build-up in the sand-pack for Na-silicate slug sizes of 0.45 and 0.5 happens at about t=200 min, in a good agreement with bulk measured

gel time (t=180 min). It takes slightly more time after gelation in sand-pack to be sensed by the pressure gauge at low injection rates. As depicted in Figure 4.35, Na-silicate slug sizes $\leq$ 0.4 cannot increase the flow resistance in the sand-pack after the gel placement, because of high water override (Figure 4.34). In the case of larger slugs of 0.45 and 0.5 PV, pressure increases after the gel setting time and then stabilizes at different values, as shown in Figure 4.35. The pressure stabilization indicates that a water communication path is formed between the two sides of the gel at about t=800 min, which cannot be detected in Figure 4.34. By increasing pressure behind the Na-silicate slug, water gradually overcomes the viscous force of the newly formed gel at the top. It was observed that water override was happening by displacement of small water droplets at the top of the formed gel. Residual resistivity factor (F_{rr}) for 0.35, 0.4, 0.45 and 0.5 PV slug sizes is 1, 1.7, 18.5 and 650, respectively. F_{rr} was determined by the relative pressure drop in the sand-pack after gel placement and before gel treatment.

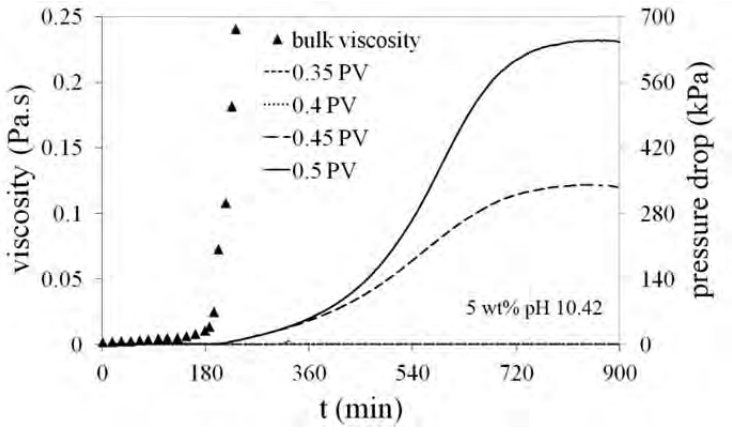

Figure 4.35. Pressure drop in sand-pack A as a function of time after placement of Na-silicate gel (5 wt% pH 10.42) at the middle of sand-pack. The results are compared for different Na-silicate slug sizes. The bulk measured viscosity for the tested Na-silicate sample is also presented.

4.3.2.3. Gel application in a dual-permeability sand-pack

The in-depth performance of Na-silicate gel is studied in this section using a dual-permeability porous medium. The experimental test is simulated using CMG (STARS). More details about the experimental setup and procedure and the employed numerical method are found in section 3.2.3. The medium is initially saturated with red dyed oil (*n*-C10 and 0.01 M NN-DMDA) and colorless irreducible SSW. It is initially flooded by 0.5 total PV of SSW with flow rate of 0.1 ml/min. During all the steps of flooding experiments, the pressure drops along both sand-packs are the same. The measured and simulated pressure drops are depicted in Figure 4.36. Pressure drop increased to about 1.5 kPa until water starts to flow through the high permeability sand-pack, then the pressure almost stabilized during water injection period, as shown in Figure 4.36. During water flooding period, water preferentially sweeps the oil in the high permeability sand-pack, while low permeability sand-pack remains unswept, except small parts close to the inlet. As shown in Figure 4.37a, the simulated pressure distributions in both sand-packs are similar during water-flooding period. However, since a given pressure drop results in a higher flow rate in high permeability sand-pack, the major oil production occurs in this sand-pack. After water breakthrough in sand-pack B, the oil production becomes negligible, while water production dominates, as shown in Figure 4.38. Water flooding oil recovery factor is less than 50%.

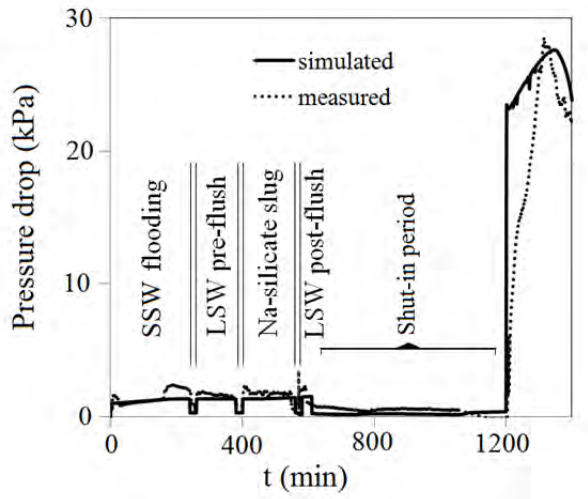

Figure 4.36. Simulated and measured pressure drops along the sand-packs during dual-permeability sand-pack flooding experiment.

Medium profile modification using Na-silicate gel was performed to recover the remaining oil in low permeability sand-pack. 0.25 PV of LSW is injected as a pre-flush to dilute the ions of SSW, in order to avoid precipitation and hence unwanted plugging. It was then followed by injecting 0.4 PV of 5 wt% Na-silicate solution with pH 10.7. Using prediction method, presented in section 4.2.2, pH is set high enough to ensure that the gelation is delayed to place the gel at the middle of sand-pack, while it mixes with LSW and becomes hot under T=50 ^{o}C. As shown in Figure 4.36, the measured pressure drop during Na-silicate injection is about 1.7 kPa (approximately 13% higher than that of water flooding), indicating good injectivity of Na-silicate prior to gelation. It is observed that the injected Na-silicate only flows through the high permeability sand-pack, except small amount which penetrates in low permeability sand-pack, mostly due to diffusion. LSW was injected afterward to displace the Na-silicate from the inlet and to dilute the Na-silicate leakoff in low permeability sand-pack. Then injection rate was reduced to 0.001 ml/min to let the gel set.

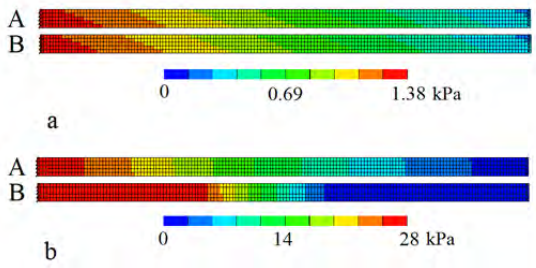

Figure 4.37. Simulated pressure distributions in sand-packs A and B during water-flooding a) before gel treatment and b) after gel treatment.

Water injection rate was increased to 0.1 ml/min at t=1200 min. Upon increasing water injection flow rate, pressure increases sharply to a higher level (Figure 4.36) and the injected water goes through the low permeability sand-pack (A) and sweeps the remaining oil, as shown in Figure 4.38. Figure 4.37b shows that pressure drops between the two ends of both sand-packs remained similar; however the pressure distributions are different. There is a high pressure behind the formed gel in sand-pack B, while there is a pressure gradient in sand-pack A, due to water flow with constant rate. Na-silicate gel treatment enhances oil recovery factor to more than 80%.

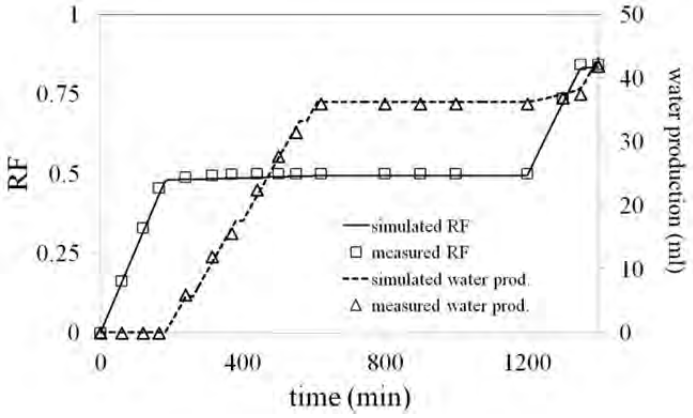

Figure 4.38. Simulated and measured oil recovery factor and water production for dual-permeability sand-pack flooding experiment.

4.3.2. Practical considerations in sodium silicate field applications

During Na-silicate in-depth treatment, it is important to avoid plugging of the oil-bearing low permeability area (matrix). It may happen by leaking off the injected solution into the matrix. The sizes of the injected Na-silicate slug and post-flush water are also important factors to make a gel with a proper length at the desired position in the reservoir. To avoid divalent ion precipitation, it is critical to inject big enough low salinity water as pre- and post-flush to separate the formation water from the injected Na-silicate. The mixing zone provided by the low salinity pre-flush is a controlling factor for the plugging time of the injected solution. The thermal gradient in the reservoir, which is formed by long-term cold water flooding, is another controlling parameter for Na-silicate in-depth gelation. Several numerical experiments are done in this section to address these practical issues, using the two-layered reservoir studied in section 4.1.2 (see Table 3.4).

A necessary step before Na-silicate field application is to run a tracer test in the sector of the reservoir which is going to be treated. The obtained field data from the tracer test gives an estimation of dispersion coefficient in the studied reservoir sector. Dispersion coefficient is important to determine the rate of Na-silicate dilution with the formation water and the length of mixing zone created by the low salinity pre-flush. A numerical simulation can be employed then to predict the placement of the gel under reservoir conditions.

Na-silicate slug size. Figure 4.39 shows the Na-silicate slug size and post-flush water amount to make a 180 ft gel at the middle of the HP layer of the studied reservoir. The results are compared for five different reservoirs, given in Table 4.2. The Na-silicate solution is injected after 1 PV water flooding. The slug sizes are reported as PV of the HP layer. The first column in Figure 4.39 shows the calculated Na-silicate and post-flush water slug sizes in the

case with no dilution or leakoff into the LP layer. Figure 4.40 illustrates the concentration ratio of the injected Na-silicate for different studied cases at three moments: the end of Na-silicate slug injection, the meanwhile to the target, at the targeted position. It is supposed that the gel is formed only when the normalized concentration of Na-silicate is higher than 0.7. This is a realistic assumption, since a practical Na-silicate content for field applications is between 4 to 5 wt% and Na-silicate never gels if it is diluted to lower than 3 wt%. The color scale in Figure 4.40 is therefore regulated to demonstrate the portion of the injected Na-silicate that is going to be gelled ($C/C_0 > 0.7$).

Table 4.2. The properties of different studied reservoirs for in-depth gel placement.

Case	**Permeability ratio**	μ_o / μ_w	$\mathbf{k_v/k_h}$	**Cross flow**
a	10	1	0.01	free
b	100	1	0.01	free
c	10	10	0.01	free
d	10	1	0.1	free
e	10	1	0.01	banned

In general, as shown in Figure 4.39, the required Na-silicate slug size for all the studied cases are at least 1.5 times of the one without dilution or leakoff. Figure 4.40 shows that the profile of the injected solution changes as it propagate in the porous media, depending on the reservoir and fluid properties. The final shape of the gel is different for the different studied cases; however, it is generally thicker at the bottom and thinner at the top, as discussed in section 4.3.1.2 for gelation in sand-packs, due to the gravity segregation effect. With this gel profile the water override is expected.

When cases (a) and (b) are compared, it can be seen that the reservoir with higher permeability ratio needs considerably less slug sizes of Na-silicate and post-flush water (Figure 4.39). As discussed earlier in section 4.1.2, as permeability ratio increases, higher proportion of the injected fluid flows through the HP layer; hence the leakoff into the LP zone is very lower, compared to a lower permeability ratio (Figure 4.40a, b). However as shown in Figure 4.40a, most of the leaked off Na-silicate in the LP zone in case (a) is diluted with the post-flush water. The small plugged area in the LP zone of case (a) after gel placement does not have considerable effect on the later water flooding performance.

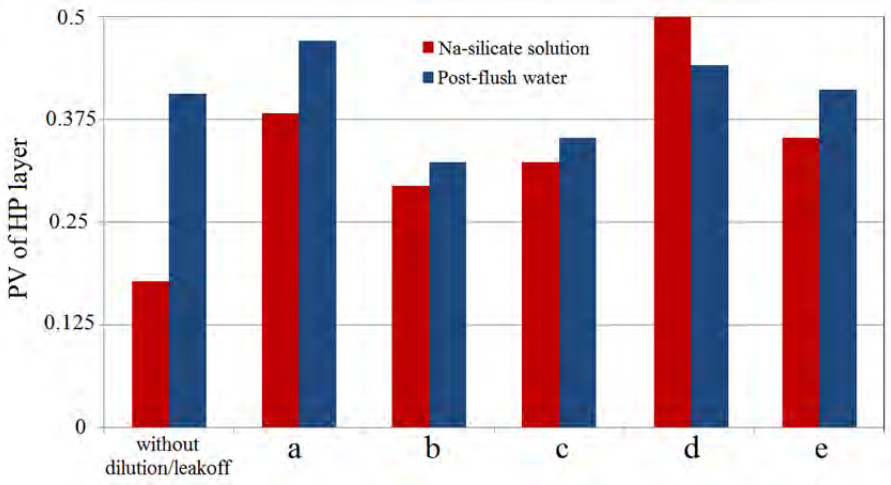

Figure 4.39. The required slug size of Na-silicate solution and post-flush water amount to place a 180 ft gel at the middle of the HP layer in the two-layered reservoir. The results are shown for different studied cases a-e, listed in Table 4.2. The first columns are devoted to the calculated values for a case without dilution and leakoff.

As viscosity ratio increases from 1 in case (a) to 10 in case (c), the required Na-silicate and post-flush slug sizes decrease. These values are relatively close to the case (b), since, as discussed in section 4.1.1, both high permeability contrast and viscosity ratio exacerbate water channeling effect,

so the injected fluids tend to flow through the HP layer with greater proportion. The penetrated Na-silicate into the LP layer is smaller in the case (c) compared to the case (a) (Figure 4.40c).

As shown in Figure 4.39, the maximum required gel slug is for case (d) which is a reservoir with high k_v/k_h. When vertical permeability is high, the flow contribution of the water channel to the LP layer is higher (Figure 4.11). Large amount of the injected fluids, including pre-gel material, leaks off to the LP layer (Figure 4.40d). So it is observed that the post-flush water could not fully dilute the leaked off Na-silicate in the LP zone. However, since the rear of the formed gel in the HP layer outruns the front of the Na-silicate leaked off volume in the LP layer, the flooded water can be diverted through this gap into the LP zone and enhance sweep efficiency. The Na-silicate slug deformation due to the gravity segregation is intensified for case (d), as shown in Figure 4.40d.

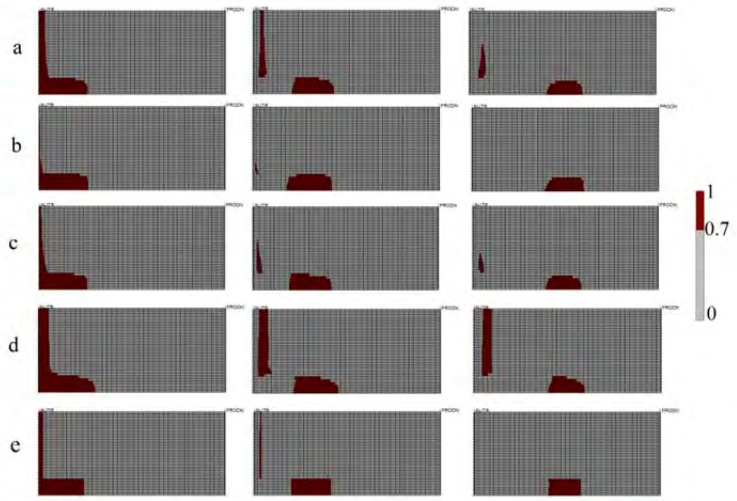

Figure 4.40. Snapshots of Na-silicate concentration ratio in the two-layered reservoir at three different moments: just after slug injection (to the left), at the midway to the target (middle) and at the targeted distance (to the right). The results are shown for different studied cases a-e, listed in Table 4.2.

As shown in Figure 4.39, the required Na-silicate is slightly less for the case (e) which is the reservoir without cross flow, compared to case (a). The water channel expansion which occurs in the case of free cross flow, discussed in section 4.1.2, results in higher Na-silicate penetration into the LP layer, especially close to the HP layer. This phenomenon is not the case in reservoir without cross flow (e), as shown in Figure 4.40e. The gravity segregation effect, which caused gel deformation in all the previous studied cases a-d, does not happen in case (e). This is mainly because the flow through the HP layer is disconnected from the gravity effect of the upper fluids in bulk of the LP layer.

As a general conclusion in this section, the problem of matrix plugging is less pronounced when the injected chemical is water-soluble, such as Na-silicate, compared to the oil-soluble materials. Since the injected aqueous chemical which has been leaked off into the matrix will be dispersed to some extent by the post-flush water. However, due to the same reason, to plug a certain volume of the HP layer, it is always necessary to inject a greater volume of the water-soluble chemical, compared to oil-soluble ones.

LSW pre-flush mixing zone. A numerical study is done on case (a), see Table 4.2, to show the importance of LSW pre-flush in diluting the ions in formation water before Na-silicate injection. LSW pre-flush is to avoid metal silicate precipitation. It can be also used to control the plugging time.

It is assumed that the reservoir initial water and the flooded water are sea water, while the pre-flush is LSW (4% salinity of sea water). Na-silicate solution is injected into the reservoir after 1 PV reservoir water flooding. The slug size of the Na-silicate solution is 0.45 PV of the HP layer. Two different pre-flush sizes, case 1 and case 2, are compared in this study. The pre-flush size is 0.09 and 0.18 PV of the HP layer for cases 1 and 2, respectively. Figure

4.41 is a dimensionless graph showing concentration ratio of the injected Na-silicate slug and the relative water salinity for the two studied cases at the bottom of the HP layer as a function of dimensionless distance (x/L), where x is distance from the injector and L is the reservoir length. The results are shown at two moments: I) after injecting 0.2 of the Na-silicate slug volume (solid lines) and II) when Na-silicate slug is placed at the middle of the medium (dashed lines). It is assumed that the relative water salinity of sea water is 1.

The Na-silicate concentration ratio of 0.75 is assumed to be the base concentration for the analysis, below which no precipitation occurs. It is also assumed that Na-silicate precipitation would not cause permeability reduction (plugging) as long as the relative water salinity is below 0.1 (Skrettingland and Stavland, 2012). As shown in Figure 4.41 at moment I, the relative water salinity in contact with Na-silicate C/C_0=0.75 is 0.06 and 0.02 for the two pre-flush cases 1 and 2, respectively. This means both pre-flushes could prevent plugging in this stage of Na-silicate injection. At moment II, the relative water salinity in contact with Na-silicate C/C_0=0.75 increases to 0.12 for pre-flush case 1, which shows the possibility of plugging due to precipitation with this size of pre-flush. Plugging at this time may be desirable, since the gel has been placed at the middle of the reservoir and precipitation enhances the residual resistance factor of the treated zone. However, pre-flush case 2 still prevents plugging in this moment, due to a thicker mixing zone.

The same study has to be done to estimate the size of LSW post-flush to avoid unwanted plugging behind the Na-silicate slug. In the case of free cross flow between layers, it is also important to take care of the water salinity in the LP layer, which is not diluted with the same rate as the HP layer. It may cause plugging in the contact area between the HP and the LP layers.

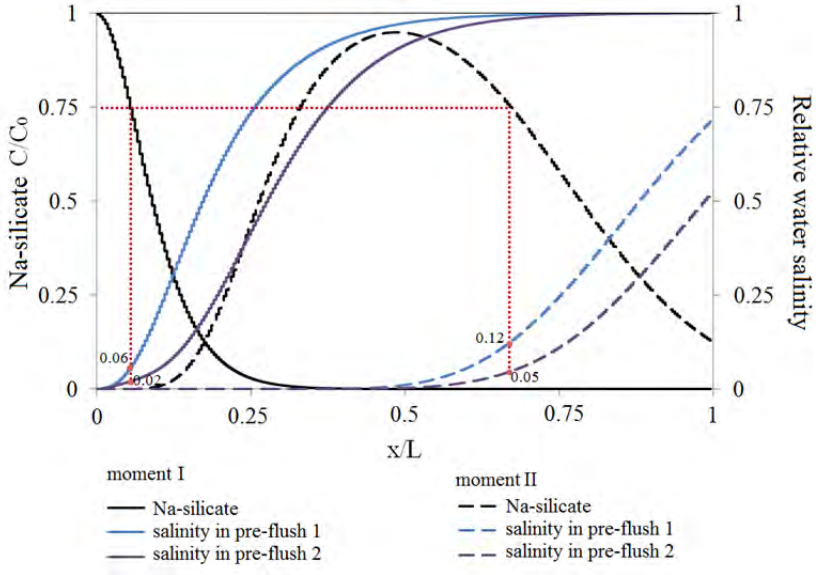

Figure 4.41. Concentration ratio of the Na-silicate slug and the relative water salinity as functions of normalized distance into the reservoir. The results are shown for two different LSW pre-flush cases 1 and 2 and at two different moments I and II during Na-silicate placement.

Reservoir thermal front. Figure 4.42 shows the reservoir temperature and Na-silicate slug transportation in the bottom of the HP layer as functions of the normalized distance, at the same moments I and II in the previous study. Reservoir initial temperature was 120 ^{o}C, which has been cooled by 1 PV water flooding with temperature of 18 ^{o}C. The main temperature decrease happens through the HP layer, where the major water has been flooded. There is a temperature gradient from 18 ^{o}C close to the injector to about 70 ^{o}C close to the producer in the HP layer.

The injected slug of Na-silicate is therefore heated up as it transports in the medium. Higher temperatures accelerate the gel setting time. So the temperature gradient could be a controlling factor for the gel placement in the desired position. As the reservoir goes to a shut-in mode after Na-silicate

placement, the HP layer warms up to some degrees (approximately 5 ^{o}C after 4 months shut-in), as depicted in Figure 4.42. The temperature increase during shut-in period helps faster gelation of the in-placed Na-silicate.

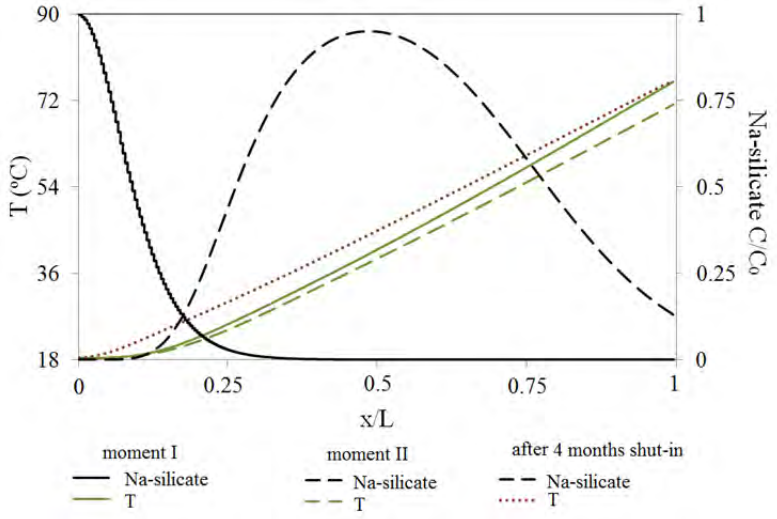

Figure 4.42. The concentration ratio of the injected Na-silicate slug and the HP layer temperature as functions of normalized distance into the reservoir. The results are shown at two different moments I and II during Na-silicate placement and after 4 months of reservoir shut-in.

5. CONCLUSIONS AND FUTURE WORKS

In this section, the overall conclusions from this study are addressed. Recommendations for the future work are also suggested.

5.1. Conclusions

Gelation time, gel strength and shrinkage are the major parameters that affect the application of a gel for in-depth treatments to increase flow resistance in high permeability zones of the reservoir. These parameters were studied quantitatively for alkaline sodium silicate system under the effects of different factors, including the silicate content (wt%), the pH, the formation water salinity especially divalent metal ions and the temperature.

In general, each factor that accelerated the gel setting time resulted in a stronger gel and a higher rate of gel shrinkage. However, temperature accelerated the gel time while the gel strength was reduced when temperature increased from 20 to 50°C. Further increase in the temperature to 80°C showed a slight increase of the gel strength. This observation may be explained by the increase of SiO_2 solubility at higher temperatures which may cause a reduction in the pH. This in turn reduces gelation time and thereby increases gel strength compared with its level at 50°C, and causes also an early start to syneresis and greater shrinkage.

Divalent ions, such as Ca^{2+} and Mg^{2+}, decreased the gel time and increased the gel strength and shrinkage. In the case of a Na-silicate content of 4.5 wt%, a pH of 10.3 and a temperature of 20°C, for example, the gel strength was increased by a factor of about 3 and roughly 8 times faster at a combined ion concentration of 0.009 M than the solution free of divalent ions. No precipitation was observed in the case of low-salinity water (25 times diluted

sea water), which makes it a possible option for a pre-flushing fluid in the field applications.

High shear rates before the gel time, even for a short interval, accelerated the setting time. This resembles the wellbore case, and must therefore be considered in field application. High shear rates after the gel time disturbed the gel formation process and resulted in a secondary gelation at a later time.

Several flooding experiments were performed using unconsolidated sand cores to study the behavior of sodium silicate in porous media. Dynamic adsorption of silicate on the quartz surfaces was considerably lower than the estimated mono-layer adsorption. It was also demonstrated that the silicate adsorption is a reversible process, where most of the adsorbed mass is desorbed in the post-flush water. Sodium silicate showed water-like injectivity during injection in porous media, after pH adjustment and prior to gelation. It enhanced water sweep efficiency in a dual-permeability sand-pack system, without affecting the productivity of the low permeability medium.

Some of the main considerations for field application of sodium silicate were addressed using numerical simulations. It was demonstrated that the reservoir and fluid properties - such as permeability ratio, viscosity ratio, vertical permeability and cross flow- have to be considered in designing an in-depth treatment. The mixing zone resulted from low salinity pre-flush and the temperature gradient resulted from long-term cold water flooding are the two factors which could be considered as the controlling factors for sodium silicate in-depth gelation.

5.2. Future works

This research work produced interesting outcomes that worth looking further into in the future. It would be interesting to study the behavior of sodium silicate during application in a real reservoir sector using the obtained experimental and numerical results. A reservoir pilot test provides better understanding of the limitations and considerations of sodium silicate field application.

6. REFERENCES

Akhlaghi Amiri, H.A., Hamouda A.A., 2012. Pore-scale simulation of coupled two-phase flow and heat transfer through dual-permeability porous medium. COMSOL Conference, Milan, Italy, October 10-12.

Akhlaghi Amiri, H.A., Hamouda A.A., 2013. Evaluation of level set and phase field methods in modeling two phase flow with viscosity contrast through dual-permeability porous medium. Int. J. Multiphase Flow 52, 22-34.

Akhlaghi Amiri, H.A., Hamouda A.A., 2014. Pore-scale modeling of non-isothermal two phase flow in 2D porous media: Influences of viscosity, capillarity, wettability and heterogeneity. Int. J. Multiphase Flow 61, 14-27.

Al-Dhafeeri, A. M., Nasr-El-Din, H.A., Al-Harith, A.M., 2008. Evaluation of rigless water shutoff treatments to be used in carbonate reservoir in Saudi Arabia. SPE 114331 Proceedings of Gas Technology Symposium; CIPC/SPE: Calgary, Alberta, CA, June 16–19.

An-Pang, T., 1963. Theory for polymerization of silica acid. Scientia Sinica, 9, 1311–1320.

Badalassi, V.E., Cenicerob, H.D., Banerjee, S., 2003. Computation of multiphase systems with phase field models. J. Comput. Phys. 190, 371-397.

Bai, B., Liu, Y., Coste, J.P., Li, L., 2007. Preformed particle gel for conformance control: Transport mechanism through porous media. SPE Res. Eval. & Eng. 176-184.

Baker, W.V., 1982. Grouting in Geothermal Engineering. Am. Civil. Eng., New York, USA.

Bauer, S., Gronewald, P., Hamilton, J., Mansure, A., 2004. Comments on high-temperature plugs: Progress report on polymers and silicates. Transactions, 28, 145-152.

Bauer, S., Gronewald, P., Hamilton, J., Laplant, D., Mansure, A., 2005. High-temperature plug formation with silicates. SPE International Symposium on Oilfield Chemistry, Houston, USA.

Børeng, R., Svendsen, O.B., 1997. A successful water shutoff. A case study from the statfjord field. SPE 99848 Proceedings of Production Operation Symposium, Oklahoma city, OK, USA, March 9–11.

Brinker, C.J., Scherer, G.W., 1990. Sol-gel science: The physics and chemistry of sol–gel processing. Academic Press Inc., San Diego, CA, USA.

Brown, C.E., Neustadter, E.L., 1980. The wettability of oil/water/silica systems with reference to oil recovery. J. Can. Pet. Tech. 19 (3), 100-110.

Bryant, S.L., Rabaioli, M.R., Lockhart, T.P., 1996. Influence of syneresis on permeability reduction by polymer gels. J. SPE Prod. & Facilities 11 (4), 209–215.

Burns, L.D., Burns, M., Willhite, P., McCool, S., Lawrence, K.S., Oglesby, K., Glass, J., 2008. New generation silicate gel system for casing repairs and water shutoff. SPE/DOE Improved Oil Recovery Symposium, Tulsa, OK, USA.

Cahn, J.W., Hilliard, J.E., 1958. Free energy of a nonuniform system. J. chem. Phys. 28 (2), 258-267.

Campbell, T.C., 1977. A comparison of sodium orthosilicate and sodium hydroxide for alkaline waterflooding. SPE 47th Annual California Regional Meeting of AIME, Bakersfield, California, USA.

Cole, R.C., Smith, C.W., 1978. Two water control sealant systems for matrix and channel plugging. 7th Annual Convention of Indonesian Petroleum Association, Jakarta. Indonesia.

Cole, R.C., Mody, B., Pace, J., 1981. Water control for enhanced oil recovery. European Offshore Conference, 81.

Coll, C., Muggeridge, A.H., Jing, X.D., 2001. Regional upscaling: a new method to upscale waterflooding in heterogeneous reservoirs for a range of capillary and gravity effects. SPE J. 6 (3), 299-310.

COMSOL Multiphysics User's Guide, 2011. Version 4.2, COMSOL Inc.

Dai, C., You, Q., Zhao, L. F., Xiong, W., 2010. Study and field application of profile control agent in high temperature and high salinity reservoir. SPE Trinidad and Tobago Energy Resources Conference, Port of Spain, Trinidad.

Eitel, W., 1954. The physical Chemistry of the Silicates. University of Chicago Press, USA.

Eitel, W., 1964-1975. Silicate Sciences. Vol. I-VI, Academic Press., New York, USA.

Eoff, L., Dalrymple, D., Everett, D., Vasquez, J., 2007. Worldwide field applications of a polymeric gel system for conformance applications. SPE Prod. Operat. 22 (2), 231-236.

Falcone, J.S., 1982. Soluble Silicates. ACS Symposium Series, Vol. 194, ACS, Washington, USA.

Ferer, M., Ji, C., Bromhal, G.S., Cook, J., Ahmadi, G., Smith, D.H., 2004. Crossover from capillary fingering to viscous fingering for immiscible unstable flow: experiment and modeling. Phys. Rev. E 70, 016303.

Ferguson, J., Applebey, M.P., 1930. The syneresis of silica gel. Trans. Faraday Soc. 26, 642-655.

Fletcher, A.J.P., Flew, S., Forsdyke, I.N., Morgan, J.C., Rogers, C., Suttles, D., 1992. Deep diverting gels for very cost-effective waterflood control. J Pet. Sci. Eng. 7, 33-43.

Flock, D.L., Le T.H., Gibeau J.P., 1986. The effect of temperature on the interfacial tension of heavy crude oils using the pendent drop apparatus. J. Can. Pet. Tech. 25 (2), 72-77.

Frampton, H., Morgan, J.C., Cheung, S.K., Chang, K.T., 2004. Development of a novel waterflood conformance control system. SPE/DOE 14th Symposium on Improved Oil Recovery, Tulsa, OK, USA.

Frette, O.I., Maløy, K.J., Schmittbuhl, J., Hansen, A., 1997. Immiscible displacement of viscosity-matched fluids in two-dimensional porous media. Phys. Rev. E55 (3), 2969–2975.

Green, D.W., Willhite, P.G., 1998. Enhanced Oil Recovery. SPE Textbook Series. Volume 6.

Hamouda A.A., Akhlaghi Amiri, H.A., 2014. Factors affecting alkaline sodium silicate gelation for in-depth reservoir profile modification. Energies, 7 (2), 568-590.

Hamouda, A.A., Alipour Tabrizy, V., 2013. The effect of light gas on miscible CO2 flooding to enhance oil recovery from sandstone and chalk . J. Pet. Sci. Eng., 108, 259-266.

Hardy, M., Botermans, W., Hamouda, A., Valdal, J., Warren, J., 1999. The first carbonate application of a newly developed organically cross-linked

water shutoff polymer. International Symposium on Oilfield Chemistry, Huston, TX, USA.

Hassanizadeh, M., Gray, W., 1987. High velocity flow in porous media. Transp. Porous Med. 2, 521-531.

Hauser, E.A., 1955. Silicic Sciences. Van Nostrand Publ., Prinston, USA.

He, Q., Hasegawa, Y., Kasagi, N., 2010. Heat transfer modelling of gas-liquid slug flow without phase change in a micro tube. Int. J. Heat Fluid Flow 31, 126-136.

Herring, G.D., Milloway J.T., Wilson, W. A., 1984. Selective gas shut-off using sodium silicate in the Prudhoe Bay field, UK. SPE 12473 Formation Damage Control Symposium; SPE: Bakersfield, CA, February13–14.

Hiemenz, P.C., 1977. Principles of colloid and surface chemistry. Marcel Dekker Inc.; New York, USA.

Holmes, H.N., Kaufmann, W.K., Nicholas, H.O.J., 1919. The vibration and syneresis of silicic acid gels. Am. Chem. Soc., 41, 1329-1336.

Hurd, C.B., 1938. Theories for Mechanism of the Setting of Silicic Acid Gels Chem. Rev., 22, 403–422.

Hurd, C.B., Pomatti, R.C., Spittle, J.H. and Alois, F.J., 1944. Studies on Silicic Acid Gels. XV. The Effect of Temperature upon the Time of Set of Alkaline Gel Mixtures, J. ACS, 66, 388.

Iler, R.K., 1955. The Colloid Chemistry of Silica and Silicate. Cornell University Press, Ithaca.

Iler, R.K., 1979. The chemistry of silica, solubility, polymerization, colloid and surface properties and biochemistry; John Wiley-Interscience Publ., New York, USA.

Islam, M.R., Farouq Ali, S.M., 1993. Use of silica gel for improving waterflooding performance of bottom-water reservoirs. J. Pet. Sci. Eng. 8, 303-313.

Jacqmin, D., 1999. Calculation of two-phase Navier-Stokes flows using phase field modeling. J. Comput. Phys. 155, 96-127.

Jones, P.W., Baker, R.O., 1992. Profile control in Virginia Hills EOR injectors. SPE/DOE Symposium on Enhanced Oil Recovery, Tulsa, OK, USA.

Jurinak, J.J., Summers, L.E., 1991. Oilfield applications of colloidal silica gel. J. SPE Prod. Eng. , 6 (4), 406-412.

Jurinak, J.J., Summers, L.E., Bennett, K.E., 1991. Laboratory testing of colloidal silica gel for oilfield applications. SPE, Richardson, TX, USA.

Kabir, A.H., 2001. Chemical water & gas shutoff technology- An overview. SPE Asia Pacific Improved Oil Recovery Conference, Kuala Lumpur, Malaysia.

Kennedy, H.T., 1936. Chemical methods for shutting off water in oil and gas wells. AIMEE, 118, 177-186.

Kortekaas, T.F.M., 1985. Water/oil displacement characteristics in cross-bedded reservoir zones. SPE J. 25 (6), 917-926.

Kosztin, B., Palasthy, G., Udvari, F., Benedek, L., Lakatos, I., Lakatos-Szabo, J., 2002. Field evaluation of iron hydroxide gel treatments. SPE 13th European Petroelum Conference, Aberdeen, UK.

Kristensen, R., Lund, T., Titove, V.I., Akimov, N.I., 1993. Laboratory evaluation and field tests of a silicate gel system aimed to be used under North Sea conditions. Proceedings of 7th European IOR Symposium, Moscow, Russia, October 26-29.

Krumrine, P.H., 1982. Sodium silicate in Chemical flooding processes for recovery of crude oil. Falcone J. S., Soluble Silicates, ACS Symposium Series, 194, 187-214, ACS, Washington.

Krumrine, P.H., Boyce, S.D., 1985. Profile modification and water control with silica gels. SPE 13578 Proceedings of SPE International Symposium on Oilfield and Geothermal Chemistry, , Phoenix, Arizona, USA, April 9–11.

Lakatos, I., Munkacsi, I., Tromboczky, S., Lakatos-Szabo, J., 1990. Potential of repeated polymer well treatments. SPE European Petroleum Conference, Hague, Netherland.

Lakatos, I., Munkacsi, I., Tromboczky, S., Lakatos-Szabo, J., 1993. Potential of repeated polymer/silicate well treatments. SPE Production and Facilities, 4, 269-275.

Lakatos, I., Lakatos-Szabo, J., 1996. A novel well treatment method based on in-situ hydrolysis and flocculation of inorganic compounds. SPE/DOE 10th IOR Symposium, Tulsa, OK, USA.

Lakatos, I., Lakatos-Szabo, J., Kosztin, B., Palasthy, G., 1998. Restriction of gas coning by a novel gel/foam technique. SPE/DOE IOR Symposium, Tulsa, OK, USA.

Lakatos, I., Lakatos-Szabo, J., Tiszai, G., Kosztin, B., Palasthy, G., Tromboczky, S., Bodola, M., Patterman-Farkas, G., 1999. Application of silicate-based well treatment techniques at the Hungarian oil fields. SPE Annual Conference and Exhibition, Huston, USA.

Lakatos, I., Lakatos-Szabo, J., Kosztin, B., Palasthy, G., Kristof, P., 2002. Application of iron hydroxide-based well treatment technique at the Hungerian oil fields. SPE/DOE 12th IOR Symposium, Tulsa, USA.

Lakatos, I., Medic, B.; Basic, I., Lakatos-Szabo, J., 2009. Prevention of vertical gas flow in a collapsed well using silicate polymer urea. SPE 121045 Proceedings of SPE International Symposium on Oilfield Chemistry, Woodlands, Texas, USA, April 20–22.

Lakatos, I., Lakatos-Szabo, J., 2012. Reservoir conformance control in oilfields using silicates: State-of-the-arts and perspectives. SPE Annual Technical Conference and Exhibition, San Antonio, Texas, USA.

Lake, L.W., 1989. Enhanced Oil Recovery. Englewood Cliffs, New Jersey: Prentice Hall, Inc.

Lane, R.H., Seright, R.S., 2000. Gel water shutoff in fractured or faulted horizontal wells. SPE/ Petroleum Society of CIM International Conference on Horizontal Well Technology, Calgary, Alberta, Canada.

Larrondo, L.E., Urness, C.M., Milosz, G.M., 1985. Laboratory evaluation of sodium hydroxide, sodium orthosilicate and sodium metasilicate as alkaline flooding agents for a western Canada reservoir. SPE International Symposium on Oilfield and Geothermal Chemistry, Phoenix, Arizona, USA.

Lenormand, R., Touboul, E., Zarcone, C., 1988. Numerical models and experiments on immiscible displacement in porous media. J. Fluid Mech.189, 165–187.

Liang, J., Lee, R.I., Seright, R.S., 1993. Gel placement in production wells. SPE Prod. Facil, 8 (4), 267-284.

Liu, Y., Bai, B., Shuler, P.J., 2006. Application and development of chemical-based conformance control treatments in China oil fields. SPE/DOE Symposium on Improved Oil Recovery, Tulsa, OK, USA.

Lund, T., Kristensen, R., 1993. Qualification program for deep penetration gels: from laboratory to field. IEA Workshop and Symposium on EOR, Salzburg, Austria.

Lund, T., Berge, H.I., Espedal, S., Kristensen, R., Rolfsvåg, T.A., Strømsvik, G., 1995. The technical performance and results from a large scale Na-silicate gel treatment of a production well on the Gullfaks field. 8th European Symposium on IOR, Vienna, Austria.

Mack, J.C., Smith, J.E., 1994. In-depth colloidal dispersion gels improved oil recovery efficiency. SPE/DOE 9th Symposium on Improved Oil Recovery, Tulsa, OK, USA.

Manrique, E.J., Muci, V.E., Gurfinkel, M.E., 2007. EOR Field Experiences in Carbonate Reservoirs in the United States. SPE Res Eval. & Eng. 10 (6): 667-686.

Merrill, R.C., Spencer, R.W., 1950. Gelation of Sodium Silicate: Effect of Sulfuric Acid, Hydrochloric Acid, Ammonium Sulfate and Sodium Aluminate. J. Phys. Chern., 54, 806.

Mills, R.V.A., 1922. Process of excluding water from oil & gas wells. US Patent 1,421,706.

Moradi-Araghi, A., Bjornson, G., Doe, P.H., 1993. Thermally stable gels for near/wellbore permeability contrast corrections. SPE Adv. Tech. Series 1, 140-145.

Moradi-Araghi, A., 1994. Application of low toxicity cross-linking in production of thermally stable gels. SPE/DOE 9th Symposium on Enhanced Oil Recovery, Tulsa, OK, USA.

Morganthaler, L.N., Schultz, H.A., 1994. A novel process for profile control in thermal recovery projects. SPE Annual Technical Conference and Exhibition, New Orleans, USA.

Morrow, N.R., 1990. Wettability and its effects on oil recovery. J. Pet. Tech. 42, 1476–1484.

Nagra, S.S., Batycky, J.P., Nieman, R.E., Bodeux, J.B., 1986. Stability of water flood diverting agents at elevated temperatures in reservoir brines. SPE Annual Technical Conference and Exhibition, New Orleans, LA, USA.

Nasr-El-Din, H.A., Bitar, G.E., Bou-Khamsin, F.I., Al-Mulhim, A.K., Hsu, J., 1998. Field application of gelling polymers in Saudi Arabia. SPE/DOE Improved Oil Recovery Symposium, Tulsa, OK, USA.

Nasr-El-Din, H.A., Raju, K.U., Hilab, V.V., Esmail, O.J., 2004. Injection of incompatible waters as a means of water shutoff. SPE Oilfield Scale Conference, Aberdeen, Scotland.

Nasr-El-Din, H.A., Taylor, K.C. 2005. Evaluation of sodium silicate/urea gels used for water shut-off treatments. J. Pet. Sci. Eng. 48, 141-160.

Ogunberu, A.L., Asghari, K., 2006. Curtailing water production in oil wells: A case for anionic polymers. J. Pet. Sci. Eng. 50, 176-194.

Prada, A., Civan, F., Dalrymple, D., 2000. Evaluation of gelation systems for conformance control. SPE IOR conference, Tulsa, OK, USA.

Pritchett, J., Frampton, H., Brinkman, J., 2003. Field application of a new in-depth waterflood conformance improvement tool. SPE International Conference on Improved Oil Recovery in Asia Pacific, Kuala Lumpur, Malaysia.

Qin, R.S., Bhadeshia, H.K., 2010. Phase field method. Mater. Sci. Tech. 26, 803-811.

Rannacher, R., 1996. A Feed-back approach to error control in finite element methods: basic analysis and examples. East-West J. Numer. Math. 4, 237–264.

Robertson, J.O., Oefelein F.H., 1967. Plugging thief zones in water injection wells. J. Pet. Tech., 19 (8), 999-1004.

Rolfsvåg, T.A., Jakobsen, S.R., Lund, T., Strømsvik, G., 1996. Thin gel treatment of an oil producer at the Gullfaks field. SPE 35548 Proceedings of SPE European Production Operations Conference & Exhibition, Stavanger, Norway, April 16-17.

Sahimi, M., 1993. Flow phenomena in rocks: From continuum models to fractals, percolation, cellular automata, and simulating annealing , Rev. Mod. Phys., 65, 1393–1535.

Schechter, R.S., 1992. Oil well stimulation. Prentice Hall Inc., New Jersey, USA.

Seright, R.S., 1988. Placement of gels to modify injection profiles. SPE/DOE Enhanced Oil Recovery Symposium, Tulsa, OK, USA.

Seright, R.S., 1995. Gel placement in fractured systems. SPE Prod. Facil., 10 (4), 241-248.

Seright, R.S., Martin, F.D., 1993. Impact of gelation pH, rock permeability, and lithology on the performance of a monomer-based gel. SPE Reservoir. Eng. 8 (1), 43-50.

Seright, R.S., Liang J., Sun, H., 1993. Gel treatments in production wells with water coning problems. In Situ, 17 (3), 243.

Seright, R.S., Liang J., 1995. A comparison of different types of blocking agents. SPE European Formation Damage Conference, Hague, Netherland.

Seright, R.S., Liang J., Sedal, M., 1998. Sizing gelant treatments in hydraulically fractured production wells. SPE Prod. Facil., 13 (4), 223-229.

Seright, R.S., Lane, R.H., Sydansk, R. D., 2003. A strategy for attacking excess water production. SPE Prod. Facil., 18 (3), 158-167.

Seright, R.S., Zhang, G., Akanni, O.O., Wang., D., 2011. A comparison of polymer flooding with in-depth profile modification. Canadian Unconventional Resources Conference, Calgary, Alberta, Canada.

Silva, L.F., Carbide, R.S., Farouq Ali, S.M., 1971. Waterflood performance in the presence of stratification and formation plugging. SPE 46th Annual Fall Meeting, New Orleans, USA.

Skrettingland, K., Stavland, A., 2012. Snorre in-depth water diversion using sodium silicate – single well injection pilot. SPE 18th Improved Oil Recovery Symposium, Tulsa, OK, USA.

Smith, L.R., Fast, C.R., Wagner, O.R., 1969. Development and field testing of large volume remedial treatments for gross water channeling. J. Pet. Tech., 21 (8), 1015-1025.

Sorbie, K., 1991. Polymer-improved oil recovery; CRC Press: Boca Raton, FL, USA.

Sorbie, K.S., Seright, R.S., 1992. Gel placement in heterogeneous systems with cross flow. SPE/DOE 18th Symposium on Improved Oil Recovery, Tulsa, OK, USA.

Sorbie, K.S., Feghi, F., Pickup, G.E., Ringrose, P.S., Jensen, J.L., 1992. Flow regimes in miscible displacement in heterogeneous correlated random fields. SPE 8th Symp. on EOR, Tulsa, Oklahoma, USA.

Sparlin, D.D., Hagen, R.W., 1984. Controlling water in producing operations: Part 4- Grouting materials and Techniques, World Oil, 6, 149.

STARS User's Guide, 2010. Advanced process and thermal reservoir simulator. Computer Modelling Group (CMG).

Stavland, A., Jonsbråten, H., Vikane, O., Skrettingland, K., 2011a. In-depth water diversion using sodium silicate on Snorre- fators controlling in-depth placement. SPE European Formation Damage Conference, Noordwijk, Netherland.

Stavland, A., Jonsbråten, H., Vikane, O., Skrettingland, K., Fischer H., 2011b. In-depth water diversion using sodium silicate. Proceedings of 16th European Symposium on Improved Oil Recovery; Cambridge, UK.

Sydansk, R.D., 1990. A newly developed chromium (III) gel technology. SPE Reservoir Eng., 5 (3), 346-352.

Sydansk, R.D., 1993. Acrylamide-polymer/chromium (III)-carboxylate gels for near wellbore matrix treatments. SPE/DOE Improved Oil Recovery Symposium, Tulsa, OK, USA.

Sydansk, R.D., 2007. Polymers, Gels, Foams and Resins. In Lake, L. W. (ed.), Petroelum Engineering Handbook, V(B), 13, 1149-1260, SPE, Richardson, USA.

Sydansk, R.D., Romero-Zenom, L., 2011. Reservoir conformance improvement. SPE, Richardson, USA.

Sydansk, R.D., Southwell, G.P., 2000. More than 12 years' experience with a successful conformance-control polymer-gel technology. SPE Prod. Facil. 15 (4), 270-278.

Vail, J.G., 1952. Soluble Silicates. Reinhold Publishing Corporation, New York, 1, 182.

Verfürth, R., 1996. A review of posterior error estimation and adaptive mesh refinement techniques. John Wiley & Sons Ltd and B.G. Teubner. ISBN-10: 0471967955, ISBN-13: 978-0471967958.

Verfürth, R., 1998. A posteriori error estimators for convection-diffusion equations. Numer. Math. 80, 641–663.

Vinot, B., Schechter, R.S., Lake, L.W.J., 1989. Formation of water soluble silicate gels by the hydrolysis of a diester. SPE Reservoir Eng. 4 (3), 391–397.

Vizika, O., Lombard, J.M., 1996. Wettability and spreading: two key parameters in oil recovery with three-phase gravity drainage. SPE Reservoir Eng., 11, 54–60.

Weber, K.J., 1982. Influence of common sedimentary structures on fluid flow in reservoir models. J. Pet. Tech. 34 (3), 665-672.

Wheeler, A.A., Ahmad, N.A., Boettinger, W.J., Braun, R.J., McFadden, G.B., Murray, B.T., 1995. Recent developments in phase-field models of solidification. Adv. Space Res. 16 (7), 163-172.

Yue, p., Feng, J.J., Liu, C., Shen, J., 2004. A diffuese interface method for simulating two-phase flows of complex fluids. J. Fluid Mech. 515, 293-317.

Yue, P., Zhou, C., Feng, J.J., Ollivier-Gooch, C.F., Hu, H.H., 2006. Phase-field simulations of interfacial dynamics in viscoelastic fluids using finite elements with adaptive meshing. J. Comput. Phys. 219, 47–67.

Zaitoun, A., Kohler, N., Guerrini, Y., 1991. Improved polyacrylamide treatments for water control in producing wells. J. Pet. Tech.,43 (7), 862-867.

Zhang, H., Bai, B., 2010. Preformed particle gel transport through open fractures and its effect on water flow. SPE improved Oil Recovery Symposium, Tulsa, OK, USA.

Zhang, C., Oostrom, M., Wietsma, T.W., Grateand, J.W., Warner, M.G. 2011. Influence of viscous and capillary forces on immiscible fluid displacement: pore-scale experimental study in a water-wet micro-model demonstrating viscous and capillary fingering. Energy & Fuels, 25 (8), 3493-3505.

Zhou, C., Yue, P., Feng, J.J., Ollivier-Gooch, C.F., Hu, H.H., 2010. 3D phase-field simulations of interfacial dynamics in newtonian and viscoelastic fluids. J. Comput. Phys. 229, 498–511.

Zhuang, Y., Pandey, S.N., McCool, C.S., Willhite, G.P., 1997. Permeability modification using sulfomethylated resorcinol/formaldehyde gel. SPE International Symposium on Oilfield Chemistry, Huston, TX, USA.

Papers

Papers are not included in UiS Brage due to copyright.

Evaluation of level set and phase field methods in modeling two phase flow with viscosity contrast through dual-permeability porous medium.

H. A. Akhlaghi Amiri and A. A. Hamouda

International Journal of Multiphase flow, 2013. 52, 22-34.

Paper I

Pore-scale modeling of non-isothermal two phase flow in 2D porous media: Influences of viscosity, capillarity, wettability and heterogeneity

Paper II

H. A. Akhlaghi Amiri and A. A. Hamouda

International Journal of Multiphase flow, 2014. 61, 14-27.

Paper III

Factors affecting alkaline sodium silicate gelation for in-depth reservoir profile modification.

A. A. Hamouda and H. A. Akhlaghi Amiri

Energies,2014. 7 (2), 568-590.

Pore-scale simulation of coupled two-phase flow and heat transfer through dual-permeability porous medium.

H. A. Akhlaghi Amiri and A. A. Hamouda

Presented at 2012 COMSOL Conference, Milan, Italy, October 10-12.

Paper IV

Paper V

Sodium silicate behavior in porous media being applied for in-depth profile modifications

H. A. Akhlaghi Amiri, A. A. Hamouda, A. Roostaei

Submitted to the journal of *Energies*.